Solid Earth Discuss., https://doi.org/10.5194/se-2017-91
Manuscript under review for journal Solid Earth
Discussion started: 23 August 2017

Solid Earth Discussions
Open Access
EGU

Multiphase Boudinage: a case study of Amphibolites in Marble in the Naxos Migmatite core

Simon Virgo[1], Christoph von Hagke[1], Janos L. Urai[1]

[1]Geologie –Endogene Dynamik, RWTH Aachen University, 52064 Aachen, Germany

Correspondence to: Simon Virgo (s.virgo@ged.rwth-aachen.de)

Abstract

In multiply deformed terrains, multiphase boudinage should be common, but identification and analysis of these is difficult. Here we present an analysis of multiphase boudinage and fold structures in deformed amphibolite layers in marble from the migmatitic center of the Naxos metamorphic core complex. Reconstruction of multiple boudinage generations is possible due to the exceptional 3D outcrop conditions. We identify five distinct generations of boudinage, reflecting the transition from high-strain - high-temperature ductile deformation to medium to low strain brittle boudins on the retrograde path during cooling and exhumation. All boudin generations indicate E-W horizontal shortening and variable directions of bedding parallel extension, evolving from subvertical extension in the earliest boudins to subhorizontal N-S extension during exhumation. Two phases of E-W shortening can be inferred, indicating E-W shortening in the Aegean before activity of the brittle North Anatolian Fault. This study highlights the wealth of information that can be gained from detailed analysis of multiphase boudinage structures.

1 Introduction

Boudins are periodic deformation structures that form in mechanically layered rocks under layer parallel extension (Ramberg, 1955). Since their earliest description (Harker, 1889; Lohest, 1909; Ramsay, 1881) and initial confusion in nomenclature of mullions and boudins, (c.f. Kenis et al., 2005; Kenis and Sintubin 2007) our understanding of these structures has greatly improved, and a taxonomy was established to describe the diversity of observed boudin structures (Goscombe et al., 2004). Although boudins are often depicted in 2-dimensions it has been recognized that in 3D boudins can be complex (Zulauf et al., 2011b). This complexity can be apparent when boudins are the result of more than one deformation event. Some multiphase structures such as mullions or bone boudins are indicative for a certain sequence of deformation (Kenis et al., 2005; Maeder et al., 2009). Similarly, Chocolate Tablet Boudins form by two phases of extension of layers in different directions (Abe and Urai, 2012; Zulauf et al., 2011a, 2011b), and have been used in some studies for the reconstruction of the deformation history of rocks (Casey et al., 1983; Reber et al., 2010). However, in the majority of studies of boudinage, examples of the different deformation events that could have resulted in a particular geometry are less obvious (Goscombe et al., 2004). Considering the number of studies that have utilized crosscutting shear zones, veins or superimposed folds for the reconstruction of multiply deformed domains, the use of polyphase boudinage for this purpose is yet not well developed. We propose that their ubiquity and rich structure (Goscombe and Passchier, 2003; Ingram and Urai, 1999; Maeder et al., 2009; Schmalholz et al., 2008; Schmalholz and Maeder, 2012; Van Noten and Sintubin, 2010; Zulauf and Zulauf, 2005) with a large spectrum of deformation mechanisms, from brittle-ductile rupture to ductile localization provide the potential for a new toolbox in structural geology.

In this study we identify five different boudinage phases in outcrop, and each phase provides insights into the rheology and metamorphic grade of formation. Based on earlier work on boudinaged pegmatite dikes in high grade marble of the migmatite core from the Naxos metamorphic dome (Schenk et al., 2007), we focus in this study on polyphase deformation

Solid Earth Discuss., https://doi.org/10.5194/se-2017-91
Manuscript under review for journal Solid Earth
Discussion started: 23 August 2017

structures in amphibolite layers in these marbles. Since the amphibolites are older than the pegmatites, they record a longer deformation history, which is reflected by more complex boudinage structures. Combining field data with microstructural analysis we link the different phases of deformation to metamorphic conditions on the retrograde path. In addition to insights into the rheological and deformational evolution of the lower metamorphic levels of the Aegean metamorphic core complex, this study may help to constrain the nature of East-West shortening of the domain, recognized by several authors (Urai et al., 1990; Ring and Layer, 2003; Jolivet and Brun, 2010; Hinsbergen and Schmid, 2012; Menant et al., 2013; Malandri et al., 2017) .

1.2 Geological Setting

The island of Naxos is located in the center of the Aegean Sea. This region has experienced back-arc-extension since the Eocene due to retreat of the Hellenic subduction zone towards the southwest (Gautier et al., 1999; Grasemann et al., 2011; Jolivet and Brun, 2010). This long-lived slab roll back makes the region one of the prime targets for understanding subduction dynamics and associated exhumation of HP and UHP rocks, as well as for understanding the evolution of metamorphic core complexes. The Cycladic islands have all undergone complex metamorphic evolution related to a lithosphere scale detachment system. The main detachment system (North Cycladic Detachment System) can be followed across the entire Aegean Sea, but is interrupted by the Mid-Cycladic Lineament north of Paros and Naxos (Walcott and White, 1998b).

Naxos is the largest of the Aegean islands and a prominent example of a metamorphic core complex (Lister et al., 1984). Situated in the footwall of the North Cycladic detachment system and exposing a rich variety in lithologies and metamorphic facies, Naxos has been the subject of multiple studies, and plays a key role for the understanding of the tectonic history of the Aegean domain (Buick, 1991; Gautier et al., 1993; Jansen, 1973; Jansen and Schuiling, 1976; Jolivet et al., 1994, 2004, 2010; Keay et al., 2001; Urai et al., 1990).

The geology of Naxos is dominated by a N-S trending elliptical structural and metamorphic dome, comprised of marble, metavolcanics, metabauxites and metapelitic schists of Permo-Triassic age (Andriessen et al., 1979) (Fig. 1).

The present-day metamorphic facies distribution is the result of at least three distinct metamorphic phases associated with Alpine deformation (Urai et al., 1990). The first metamorphic event at high pressure-low-temperature conditions is associated with top to the south shearing in the Hellenic subduction zone (D1), and formation of the Hellenides at approximately 50 Ma (Andriessen et al., 1979; Dürr et al., 1978; Urai et al., 1990; Wijbrans and McDougall, 1988). Large scale isoclinal folds and other deformation structures formed during D1 were overprinted by top to the north shearing of D2, starting at the onset of crustal thinning and post-orogenic extension in the early Miocene (Mercier et al., 1976; Ring et al., 2010; Urai et al., 1990). As a consequence of crustal thinning and extension of the Aegaen domain the rocks of Naxos were overprinted by regional scale greenschist metamorphism at ~25 Ma ($M2_a$), and more localized high temperature – low pressure metamorphism ($M2_b$) with thermal dome formation and partial anatexis at ~16 Ma (Duchene et al., 2006; Keay et al., 2001; Martin et al., 2006, 2008). The metamorphic grade of $M2_b$ decreases from a high grade migmatitic core down to greenschist facies along its fringes (Jansen and Schuiling, 1976). The estimated 50-70km top-to-North shearing of the North Cycladic detachment (Brichau et al., 2006; Jolivet et al., 2004, 2010) is reflected by a pervasive N-S lineation and shallowly dipping foliation warping around the metamorphic dome. On larger scale, N-S trending tight and isoclinal, coaxially refolded folds (B1&B2) with fold axes commonly parallelized to the N-S lineation during shearing. A late stage of upright open folds (B3) deform the axial plane foliation of B1 and B2 (Buick, 1991; Jansen, 1977; Urai et al., 1990), indicating E-W shortening. On the smaller scale D2 deformation manifests in a large variety of structures in the various metamorphic grades and lithologies. In recent years, several studies have addressed deformation structures in the high grade magmatic core, and it could be shown that structures in the migmatite dome formed through viscoplastic flow in syn-migmatic M2b conditions (Kruckenberg et al., 2010, 2011; Rey et al., 2011). In the later stages of the M2b metamorphism, pegmatite dikes intruded

Solid Earth Discuss., https://doi.org/10.5194/se-2017-91
Manuscript under review for journal Solid Earth
Discussion started: 23 August 2017

the marble (e.g. Buick 1991). The complex tectonic history is reflected in U-Pb ages from zircon in amphibolites, which show inherited old cores and two phases of later overgrowth at 40 and 15-14 Ma, respectively (Bolhar et al., 2016). These ages may be interpreted either as early intrusion, during ocenazitation of the Aegean, or as late emplacement during large-scale extension (Bolhar et al. 2016). Zircon and apatite fission track data from all tectonic units exposed on Naxos as well as U-Pb ages show a consistent cooling and exhumation scenario: cooling started at ~25 Ma, and continued until ~ 8 Ma (Seward et al. 2009, Brichau et al., 2006, John and Howard, 1995).

Structures in the central migmatite dome have been analyzed in the field and several syn-migmatic subdomes were identified (Vanderhaeghe, 2004) (Fig. 2) . Within the mantling sequence around the migmatite dome, mylonitic shear zones indicate relative upward movement of the migmatite while progressive transposition and folding of granitic dikes result from vertical flattening and top to-the-NNE shearing during dome formation (Vanderhaeghe, 2004). Outcrop-scale mapping and analysis of the magnetic fabric of the internal structure of the migmatite revealed two compartments of subdomes separated by a N-S trending high strain zone, which contains km-scale rafts of marble folded into pinched synforms (Kruckenberg et al. (2010, 2011), Figure 1). The authors conclude that an interplay between buoyancy and isostasy- dominated flow is responsible for the complex internal structure of the migmatite, and dome formation was driven by upper crustal extension and shearing with coeval lower crustal E-W convergent flow.

This paper builds on a case study which focused on deformed pegmatite dikes within marbles from the high strain zone mentioned above (Schenk et al., 2007), showing how pegmatites are affected by brittle domino boudinage. Schenk et al. (2007) proposed that Mode-I interboudin fractures formed at lithostatic fluid pressure conditions after solidification of the pegmatite. Decreasing pore fluid pressures under continuing N-S extension of the pegmatite inhibited further opening mode deformation in the inter-boudin zones and consequently the boudin blocks rotated during ongoing deformation of the surrounding marble. In this study we explore the polyphase deformation recorded in boudinaged amphibolite layers in these marbles. In addition to blocky boudinage which also occurs in the pegmatites, the amphibolite layers record higher temperature deformation, as witnessed by pinch and swell boudins. These structures have as of now not received much attention, but, as they record multiple deformation events, may provide insights into the tectonic evolution of Naxos and the Aegean.

2 Methods

The field data presented in this study was collected in active and recently abandoned marble quarries in the central hills of Naxos, in the vicinity of Kinidaros (Fig. 2). As a result of the mining activities outcrop conditions are exceptional, with large and unweathered vertical and horizontal saw cut surfaces (Fig. 3). As compared to the often heavily weathered natural outcrops of the island with only limited 3D exposure, the quarries allow for extensive high quality observations.

Orientation data was collected in situ using a Breithaupt structural compass. We use cross cutting and interaction relationships to establish a relative temporal order of the structural elements. Parts of the age relationship observations were conducted in mined blocks in the quarry. The exact origin of these blocks in the quarry is not known. However, the orientation of the blocks can be constrained, as the faces are always cut either subvertically or subhorizontally, and the orientation of the amphibolite layers and most structures was found to be consistent throughout the quarry. We used these blocks for structural analysis on five sides of the block and for sampling for microstructural analysis in plane polarized and crossed polarized transmitted light using the Virtual Petrography (ViP) microscope (Virgo et al., 2016).

3 Results

We have identified six generations of outcrop scale deformation structures in the study area (Fig. 3, 4): two generations of pinch-and- swell boudins (Fig. 5), folds (Fig. 6), and three generations of brittle boudins (domino boudins, torn boudins and

Solid Earth Discuss., https://doi.org/10.5194/se-2017-91
Manuscript under review for journal Solid Earth
Discussion started: 23 August 2017

hairline veins, Figure 7). In addition to these, the marbles are affected by late deformation structures such as rare mylonitic shear zones and brittle normal- to oblique slip faults (Fig. 5c) that have been described in detail in the marble (Schenk et al., 2005) and surrounding lithologies (Buick, 1991; Cao et al., 2017; Vanderhaeghe, 2004).

In the following we give a short overview of the bulk properties and microstructure of the marble and amphibolite before we describe the different generations of boudins and folds in more detail. For the description of the boudin structural elements and geometries we follow the terminology of Goscombe et al. (2004).

3.1 Marble

The marbles of the migmatite core are characterized by their mineralogical purity and large grain size. The bulk grain size of the marble in the study area is the largest observable on the island with grain diameters up to 20 mm (Covey-Crump and Rutter, 1989; Ebert et al., 2009).

The marbles are diffusely banded with band thicknesses of lighter and darker gray marble ranging from few centimeters up to 1.5 meters. White bands of high purity are often found adjacent to amphibolites. Around some amphibolites an orange to red iron staining of the marble from iron oxides can be observed predominantly along grain boundaries.

The bulk marble appears to have an isotropic texture; however, the quarrymen report a N-S trending vertical preferred fracturing orientation of the marble in mining operations that might indicate a grain scale anisotropy and a foliation normal CPO was reported by Ebert et al. (2009).

The dominant marble microstructure is characteristic for dynamic recrystallization at high temperature (Fig. 8): amoeboid grains with lobate grain boundaries and orientation families indicating extensive strain induced grain boundary migration. In triple junctions, angles between grain boundaries are typically at around 120 degrees. Subgrain boundaries are less common, indicating subgrain rotation.

The overall grain size distribution is heterogeneous and bimodal: The majority of grains are between 300 and 600 µm in 2D sections. Exceptionally large grains (>10mm) which occur locally in some layers are interpreted to have formed by exaggerated grain growth during dynamic recrystallization.

The vast majority of calcite grains in the marble show twinning, undulose extinction and local grain boundary migration recrystallization (in the boudin necks of domino boudins, see below) to much smaller grain size as a consequence of low-temperature deformation overprint.

3.2 Amphibolite

Amphibolite layers are by far the most common inclusion in the marbles; pegmatite dikes and bodies of felsic schists are less frequent. In the study area amphibolite layers consistently strike N-S with dips from close to vertical in some quarries and less steeply (~60°) to the East in others (Location 10-15 and 32-35, Figure 2). Spacing of the layers is in the range of tens of centimeters to several meters and their thickness is usually less than 20 cm. The bulk mineralogy of the amphibolites consists of mostly hornblende (tschermakite) and plagioclase (andesine) with muscovite, biotite, and accessorial titanite (Schenk et al., 2007). The interface of marble and amphibolite is well defined. Some layers show internal layering at the scale of a few centimeters caused by variation of plagioclase content. The foliation which is sometimes present in the amphibolites (for example in the hinges of folds) results from compositional variation and not from preferred orientation. In all thin sections the amphibolite has an isotropic texture, even in zones where high strains can be inferred (e.g. in fold hinges and in the pinches of pinch-and-swell boudins). We interpret this as an indication for static recrystallization of the amphibolite after a high strain deformation, erasing the fabric of earlier dynamic recrystallization by static grain growth (C. Passchier, personal communication). Indicators for some low strain deformation of the bulk amphibolite are minor undulouse extinction in feldspars and amphibole grains fractured along their cleavage planes.

Solid Earth Discuss., https://doi.org/10.5194/se-2017-91
Manuscript under review for journal Solid Earth
Discussion started: 23 August 2017

Nearly all amphibolite layers are boudinaged and at least five different types of boudins can be distinguished based on outcrop and thin section which are described in detail below. It is interesting to note that very thin layers of amphibolite (<5mm) only show discernible boudinage if they are very close to a thicker amphibolite layer to form harmonic boudins. If the distance is high enough, very thin amphibolite layers do not boudinage but act as passive deformation marker horizons in the marble (Fig. 7e).

3.3 Long wavelength pinch-and-swell boudins

The generation that is overprinted by all other structures is long wavelength pinch and swell boudinage (lλ). lλ can only be found in layers thicker than ~5 cm and due to the long wavelength they can best be observed and measured at large N-S trending layer parallel cuts that expose the amphibolite layer across a large area (Fig. 3c, 9). The thickness of the amphibolite is reduced to locally less than a millimeter in the pinches, but a full disruption of the amphibolite (tapering boudins) was never observed. The amphibolite exhibits an isotropic texture in both pinches and swells despite considerable strain (this indicates static recrystallization of the amphibolite after this deformation phase). The trace of the boudins (the lineation of the boudin necks (L_b), Goscombe et al., 2004) is consistently sub horizontal throughout the study area, indicating vertical extension of the layers. Wavelength λ of the boudinage correlates with amphibolite thickness and can reach several meters for amphibolites with a thickness of a few decimeters.
Estimated from the length of the pinches (M') and the thickness difference between pinches and swells (W/W'), the amount of extensional strain is at least 100%, probably several hundred percent.

3.4 Short wavelength pinch- and-swell boudins

Pinch and swell boudins with a much shorter wavelength (sλ) overprint lλ . In many layers sλ is only developed in the lλ pinches. However, clear age relationships can be observed where sλ boudins are present and well exposed in the swells as well as the high-strain pinches of lλ: in both sλ boudin necks have the same orientation, showing that sλ is clearly younger (Fig. 9). Within the same layer the wavelength of this generation is commonly less than half the wavelength of the previous lλ pinch and swell boudins. The lineation of boudin necks (L_b) is dipping shallowly to the south (20°- 45°) and intersects with the local lλ boudin necks at an angle of >20°.
The swells of sλ are mostly symmetric with convex exterior planes and can be classified as drawn boudins and tapering boudins following the classification scheme by Goscombe et al. (2004). Occasionally fish mouth terminations are found (Fig. 10c). Neither in thinned out pinches nor in strongly deformed parts of the swells we were able to identify markers for dynamic recrystallization in the amphibolite, indicating that this generation also predates the static recrystallization of the amphibolite. sλ boudins are in many cases associated with biotite that can often be found enriched in the pinches, wrapping around the outer perimeter of the boudins. The amount of extensional strain by short wavelength pinch-and-swell boudinage is with an estimated minimum of 50% considerably lower than that of the previous generation.
The general appearance of sλ boudins suggest a ductile deformation of both amphibolite and marble. However, associated with some boudins of sλ we found structures which may indicate deformation at lower temperatures:
Some highly thinned out pinches show a higher fraction of calcite grains in the amphibolite, up to the point that grains of amphibole and plagioclase are fully isolated in the marble matrix. The isolated grains have a grainsize comparable with the statically recrystallized amphibolite in the swells, which is interpreted as a granular flow deformation of the amphibolite postdating static recrystallization (Fig. 8d). This granular flow could have occurred in the final stages of sλ, or, during the domino boudin phase (see below) when amphibolite layers already thinned in the lλ, and sλ, were more susceptible to deformation.

Solid Earth Discuss., https://doi.org/10.5194/se-2017-91
Manuscript under review for journal Solid Earth
Discussion started: 23 August 2017

Furthermore, some boudins of this generation that appear as symmetric drawn boudins on first sight, exhibit localized low angle shear zones in the interboudin zones. The shear zones extend into the surrounding marble at ~30° to the layer with a microstructure analogous to domino boudins (see below).
Whether these structures have formed in the late stage of sλ or are a much younger overprint could not be resolved.

3.5 Folds

In many locations amphibolite layers are isoclinally folded, in asymmetric folds that occur in both S and Z chirality (both looking down or horizontally) (Fig. 6). Their age relationship with the pinch and swell structures is not fully resolved, but they are crosscut and displaced by domino boudins, pegmatite dikes (compare Figure 3A in Schenk et. al 2007) torn boudins and late hairline veins.
The fold axes have variable plunge to north or south. Normal to the fold axis the asymmetric folds rarely have limbs longer than 2 m. In contrast, parallel to the fold axis they extend for several tens of meters, often over multiple quarry soles. The thickness of the amphibolite in the fold hinges is strongly increased relative to the limbs. The hinges are in some locations characterized by a weak foliation fan with statically recrystallized amphibolite and thin calcite veins (Fig. 10). The foliation is often highlighted by cuspate-lobate amphibolite - marble interfaces. The cuspate-lobate structures may be the result of interface buckling during folding (Biot, 1964), however calcite inclusions in the extension of cusps in some folds suggest that they formed by shortening of a preexisting boudin generation subnormal to the shortening axis of the fold (Fig. 10d). In the field, fold hinges are often associated with an increased occurrence of biotite. In the thin sections, cuspate-lobate structures sometimes show actinolitic rims with a shape preferred orientation parallel to the interface, while the amphibolite in the cusps has an, statically recrystallized texture (Fig. 10b).
A rare variety of small scale folds are concentric open folds, these were only encountered in a single non-in situ block of marble close to Location 2 (Fig. 6a).

3.6 Brittle boudins

Brittle boudins are characterized by sharply localized fractures in the amphibolite. Due to the generally steep orientation of the brittle fractures they are much more obvious on the quarry floor then on vertical sections (Fig. 4, 7).
We differentiate three types, based on the failure mode, relative age and characteristics of the fractures: domino boudins, torn boudins and hairline veins.

3.7 Domino Boudins

Domino boudins occur in many amphibolite layers of the study area but by far not in all. They are characterized by asymmetric, rotated boudin blocks and sharply defined shear fractures. The shear fractures cut the amphibolite layers at an angle θranging from 60°- 90° (defined as the angle between the fracture and boudin interface, see Goscombe et al., 2004). On both sides of the shear fractures in the amphibolite, thin shear zones extend into the surrounding marble as zones with sharp slip planes and dramatically reduced grain size (Fig. 11, 12). With increasing distance from the amphibolite these shear zones splay and curve towards parallel to the layer which indicates a layer parallel shear component that is in line with forward vergent rotation of the boudin blocks.
The largest amount of displacement is parallel to the shear fractures (D) while dilation between the block faces (N) is generally low. The mineralogy of interboudin zones regularly contain, besides calcite, also an opaque mineral (presumably pyrite) and sheared biotite. On exposed shear fractures, a slickenside lineation is commonly present.
A full detachment of boudin blocks by large extension into asymmetric tapering boudins (Goscombe 2004) is rare in the study area; in most amphibolite layers the domino blocks are still in contact to each other.

The length to width ratio (L/W) of this generation can be as low as 1 but more commonly it is in the order of 3-5 and in extreme cases >8.

Looking down on the quarry floor, over distances up to 30 m, within one amphibolite layer the sense of block rotation and shear displacement is commonly consistent. Along one amphibolite layer, antithetic shear fractures and block rotations in the opposite sense are rare. Adjacent amphibolite layers usually show the same sense of block rotation and shear displacement. However, both senses of block rotation and shear displacement are common and these bundles of layers with the same sense of block rotation and shear displacement are usually separated by layers without domino boudins.

Domino boudin necks are highly variable in strike, due to the variation discussed above, and also due to variance in θ. Domino boudin necks have a rake between vertical and ~60° to the South.

Domino boudins consistently crosscut and displace sλ, as well as (very rarely) small-scale isoclinal fold hinges. Domino boudins are the one boudin type that can be found with similar orientation to those in the amphibolite in nearly all pegmatites (compare Schenk et al., 2007). Their formation thus postdates both Pinch-and swell generations (sλ and lλ), small-scale folding and pegmatite intrusion.

3.8 Torn boudins

Torn boudins are the second class of brittle boudins in the amphibolite. In contrast to the domino boudins, torn boudin always form in a Mode-I fracture normal to the Amphibolite layer with sharp, intra- and intergranular fractures. The main component of displacement is dilatational/normal to the fracture, however in some layers minor systematic rotation (< ~15°) of the torn boudin blocks can be observed.

In amphibolite layers that contain both torn boudins and domino boudins, the torn boudins show a lower spacing of the necks (L/W=1.5-3) than the domino boudins.

In some amphibolite layers at least 2 generations of torn boudins are present, each with a stable direction, that intersect at a low angle or form wing cracks (Virgo et al., 2013, 2014) (Fig. 9e). The rake of the older set is usually oriented subvertical while the younger set dips steeply to the south. The often times similar orientation makes age relationships of torn and domino boudins rare in outcrop. Where a clear relationship was observable the domino boudins are older than the torn boudins.

Torn boudin necks are filled with calcite and less commonly chlorite (Fig. 11). The calcite fill is blocky with grains often larger than the fracture aperture and include solid inclusion bands, indicating a cementation by precipitation. Features that would indicate an invasive flow of the surrounding marble into the opening fracture like a systematic grain size reduction in the surrounding marble or abrasion along the neck faces was never observed in thin section. However, deformation of passive markers indicate that flow of the surrounding marble into the boudin neck does play a role when the segregation of torn boudin becomes larger than a few millimeters (Fig. 7e).

3.9 Hairline veins

Hairline veins form (analog to boudins) by fracturing in layer parallel extension. The decision to call this generation of structures hairline veins rather than boudins is due to the fact that they are not strictly confined to the amphibolite but can also occur in the marble.

Hairline veins are ubiquitous in all amphibolite layers. They crosscut all other boudin and fold structures and thus represent the most recent deformation event in the amphibolite layers. Their orientation is quite stable throughout the study area dipping 60° towards the North. Hairline veins are purely opening mode veins with no signs of shear displacement. The vein cement consists mostly of chlorite and less frequently calcite.

An analog to the chlorite veins in amphibolite layers can be observed in a few locations also in the marble, confined to very pure, white bands. Nucleating preferentially at convex edges of domino boudins, chlorite filled veins extend into the

Solid Earth Discuss., https://doi.org/10.5194/se-2017-91
Manuscript under review for journal Solid Earth
Discussion started: 23 August 2017

surrounding marble above and below (Fig. 7 f). The orientation of the veins is parallel to the local chlorite filled hairline veins in the amphibolite.

Both of these veins in marble and amphibolite are parallel to the orientation of the most prominent set of large scale E-W joints and faults in the marble. The faults (Fig. 5c) can have a displacement of a few m, and they have a several m wide damage zone and a thin fault core in which open fractures are filled with fault breccia, fine grained sediment and karst deposits.

4 Discussion

Integrating the observations in several quarries allows us to interpret five distinct generations of boudinage in N-S trending subvertical amphibolite layers that record the internal deformation of the marbles from high grade M2b metamorphic conditions (lλ pinch and swell boudins) over the pro- and retrograde path (sλ pinch-and-swell boudins, domino boudins and torn boudins) to recent shallow deformation (hairline veins, joints, faults). The decrease in temperature and pressure is reflected by the embrittlement of the amphibolite and marble through the stages of deformation and by the structurally associated minerals that change from biotite to chlorite and secondary calcite.

All boudin generations indicate E-W shortening with different orientations of layer parallel extension, rotating in the plane of layering from vertical (lλ) over south vergent (sλ, Domino boudins) and horizontal (Domino boudins, torn boudins) to North vergent (Hairline veins, joints). The strains involved decrease from >>100% elongation in lλ over about 10% in domino boudins to ~1% in the hairline veins.

A compilation of our results is given in Fig. 13, relating the meso– and microstructural observations and our interpretation of the strain and temperature conditions to other structures and events. Before we discuss these results in the context of the geodynamic evolution of the Aegean, we examine aspects on our interpretation in more detail.

The origin of the amphibolite layers in the marbles is not conclusively known, but it is widely accepted that they have already existed during the high pressure metamorphism of M1 (Avigad, 1998; Bolhar et al., 2016; Buick and Holland, 1989; Martin et al., 2006). Their present day N-S trending subvertical orientation in the study area is interpreted to be a result of the high strain viscoplastic deformation during the partial melting stage of the migmatite in M2b (Kruckenberg et al., 2010, 2011; Vanderhaeghe, 2004). The marbles of our study area belong to the pinched synforms that formed in the high strain zone between the subdomes of the migmatite dome. The orientation of the amphibolites is in good correspondence to the limbs of the interpreted large scale structure in this zone. Furthermore, the long wavelength pinch and swell lλ, (the oldest boudinage structure) is consistently parallel to the axis of this pinched synform. The boudins are interpreted to have formed by (only) vertical elongation of the largescale limbs (c.f. Ramsay, 1967) during E-W shortening in M2b conditions. Considering that boudinage of the limbs first requires the formation of isoclinal folds leads to the conclusion that the amount of E-W shortening has to be much higher than what is reflected by the lλ boudins.

4.1 Folds

More work is needed to fully clarify the relative age relations of the small scale isoclinal folds. Although we know from clear overprinting relationships that they predate the pegmatite intrusion and the brittle boudinage phases, their relation to the two types of pinch-and-swell structures is not fully resolved. In some cases the folds seem to overprint the short wavelength boudins and in other cases the fold axis is parallel to the L_b of this generation which would suggest that the folds and sλ might be structurally related. Most of the observed folds are asymmetric, with changing s or z chirality and a strong variation in the dip of the fold axis. Due to this strong variation in the orientation, these folds are not directly relatable to the large pinched synform discussed above. A structural relation between folds and boudins is not uncommon: One example are the above mentioned boudins that form in the stretching limbs of isoclinal folds. In analogue studies, Zulauf and Zulauf

(2005) have described two types of symmetric open folds forming in constrictional flattening strain, the first with a fold axis parallel to the layering and the extension direction and the second with a fold axis normal to the layering, folding in-plane boudinaged sections of the stronger layer.

Very similar folds to those of our study area were described in boudinaged aplitic dikes in marble by (Poisel et al., 2016). These folds and boudins show mutual age relationships and are interpreted as coeval structures that formed in a general strain regime with components of layer parallel stretching and shear (B. Grasemann, pers. comm. 2017). The asymmetric folds in the amphibolite are generally in good correspondence with non-coaxial folds forming in simple shear and general strain regimes (Alsop and Holdsworth, 2006, 2007; Cobbold and Quinquis, 1980; Ridley, 1986). General strain conditions with pure shear and a layer parallel simple shear component may have prevailed in the marbles during some deformation stages. However, both the asymmetric folds and systematically rotated domino boudins occur in both polarities, implying that layer parallel shear is a local phenomenon and does not reflect a regionally imposed shear deformation. The possibility that s-folds are an overturned variation of z-folds (compare Llorens et al. (2013)) is considered unlikely since no indication for such high shear strains was found.

4.2 Static recrystallization

The microstructure of the amphibolite in folds and pinch and swell boudins with a lack of indicators for dynamic recrystallization suggests it has statically recrystallized. The foliation (e.g. in fold limbs) is inherited from a deformation fabric but overprinted by static grain growth so that it is at present reflected only by changes in the amphibolite composition (e.g. plagioclase content).

The static recrystallization is possibly coeval with the pegmatite intrusion in the marbles. Firstly, all statically recrystallized structures are older than the pegmatites and none is younger. Secondly, static recrystallization requires a phase of deformation quiescence which was very likely the case in this phase: The pegmatites have intruded the marble in various direction, often subparallel to the amphibolite and reactivating the heterogeneity imposed by the amphibolite (Schenk et al., 2007). This high variability in orientation requires low differential stresses, and sigma 3 approximately normal to the amphibolite layers. Low differential stress also means that there is no substantial deformation of the amphibolite which is a prerequisite for the static recrystallization. Here we speculate that this may be related to a rheological inversion in the migmatite core, when partially molten migmatite became weaker than marble.

The pegmatite intrusion and solidification and static recrystallization of the amphibolite mark the beginning of the transition from ductile deformation towards more localized brittle deformation of both amphibolites (and later also marble). This is reflected by overprinting of the short wavelength pinch-and-swell boudins by lower temperature deformation structures. Granular flow of the recrystallized amphibolite in the necks of sλ and shear zones in the marble with mechanical twins and small recrystallized grains suggest temperatures below 300ºC during deformation (Burkhard, 1993). This part of the initial retrogression was suggested to occur from 20Ma to 16.6Ma (Siebenaller et al., 2013).

4.3 E-W shortening

In the Aegean Sea, N-S to NE-SW trending fold axes indicative for E-W shortening have been found on various islands in the central Aegean, including Andros, Tinos, Mykonos, Syros, Naxos, and Paros (e.g. Angelier, 1977; Avigad et al., 2001; Gautier et al., 1993; Lecomte et al., 2010; Menant et al., 2013; Papanikolaou, 1980; Philippon et al., 2011, 2012; Urai et al., 1990). However, driving mechanisms, timing and amount of shortening in E-W direction in the Aegean remain an ongoing matter of debate, and different hypotheses have been suggested. The controversy is partly related to interpretation of the nature of the Mid Cycladic Lineament, where orientation of lineations change abruptly across a narrow zone (Walcott and White, 1998a). This may be either interpreted as strike-slip faulting associated with crustal scale shortening and block rotations (e.g. Jolivet et al., 2013; Philippon et al., 2011), or normal faulting in an overall extensional regime (Gautier et al.,

1999; Hinsbergen and Schmid, 2012) including vertical axis rotations in the footwall (Malandri et al., 2017). Field evidence is controversial, as there seems neither support for a major detachment (Brun et al., 2016; Jolivet et al., 2015; Philippon et al., 2014), nor is strike-slip faulting observed on Paros, where the Mid Cycladic Lineament might be exposed (Malandri et al., 2017; Walcott and White, 1998a). Additional complexity is added due to interaction of slab roll-back with westward migration of the Anatolian Plate since ~11 Ma (Jolivet et al., 2013; Ring et al., 2010). It has been suggested the Anatolian Plate is a main driver for observed E-W shortening, rendering the structures dominantly young if considering activity of the North Anatolian Fault (e.g. Menant et al., 2013). Earlier E-W shortening in the Aegean may be explained by the proto-North Anatolian Fault, as witnessed by ductile shearing in Turkey, that might have been linked to activity along the Mid Cycladic Lineament (Philippon et al., 2014 and references therein). Alternatively, E-W shortening may be partly independent of the North Anatolian Fault and related to crustal attenuation and viscoplastic deformation during upward flow and partial melting of the crust and mantle in an overall extensional regime (Kruckenberg et al., 2010, 2011; Malandri et al., 2017). This scenario does not exclude late-stage shortening related to movement of the North Anatolian Fault, but most strain is accommodated earlier, locally constrained to the thermal domes.

On Naxos, there is evidence for two phases of E-W shortening. The oldest boudinage structures (lλ pinch and swell structures), which take up most of the strain show vertical extension direction. This fits with the model of a pinched synform in between subdomes in the migmatite (Kruckenberg et al., 2011). In this model, E-W shortening is related to upper crustal extension and lower crustal convergent flow, and has been associated with M2b metamorphism. This so-called viscous collision does not require plate convergence, when domes form by upward rotation of horizontal deep crustal flows during crustal extension (Kruckenberg et al., 2011; Rey et al., 2011). This model implies that most of E-W shortening observed in the area is relatively old, much older than activity of the brittle North Anatolian Fault. During this deformation phase, viscoplastic flow is the dominant deformation process, driven by buoyancy and isostatic equilibration, so that no high differential stress is required to form the observed structures. Short wavelength pinch and swell boudinage (sλ) accommodate less strain that lλ, and it is not clear whether they formed during or past peak metamorphism. However, they also formed during dominant viscoplastic deformation, i.e. during an early phase of E-W-shortening.

Younger structures mapped in the amphibolite, in particular all brittle boudin types as well as the open B3 folds outside the migmatite described in Urai et al. (1990) show N-S stretching and shortening in E-W direction. All these structures formed post peak M2, thus on the retrograde path (see above). These structures are possibly linked with compression due to the North Anatolian Fault. This hypothesis could be tested for instance by dating minerals in the respective boudin necks. However, we note that the brittle structures only accommodate a small fraction of total strain in the amphibolite.

In summary, independent of local or regional importance of the signal the E-W shortening history of Naxos requires two distinct and temporally separated E-W shortening phases. The first phase between 16 and 20 Ma is dominated by viscoplastic flow and accommodates most of the total strain. After this deformation phase the amphibolite shows static recrystallization, implying little or no deformation. At a late stage, possibly related to movement of the North Anatolian Fault after 11 Ma, brittle boudins and open folds form. Episodic deformation in the Aegean is corroborated by $^{40}Ar/^{39}Ar$ geochronology, showing different structures were active at distinctly different times (Forster and Lister, 2009).

5 Conclusions

The internal deformation history of high grade marble bodies in the migmatitic center of the Naxos metamorphic dome is recorded by multiphase boudinage and folding of amphibolite layers. We identified five generations of boudins with age relationships and orientations consistent across different marble bodies in the migmatite complex. The boudin generations are from oldest to youngest: two generations of pinch-and-swell boudins, the first with a longer and the second with a shorter

wavelength. These are followed by domino boudins, torn boudins and hairline veins reflecting embrittlement of the amphibolite layers. Outcrop scale asymmetric folds predate torn boudins and hairline veins. Folds and domino boudins occur in both chiralities and indicate locally deviating shear sense. The Long wavelength pinch-and-swell boudins is consistent with the surrounding synmigmatic flow deformation structures. The timing and nature of static recrystallization in the amphibolite therefore remains elusive: If static recrystallization coincided with peak M2b, both pinch and swell boudinage phases and folds must have formed on the prograde path of M2b. This implies that main deformation in the marbles occurred before the high internal deformation of the migmatite. Alternatively, if strong deformation in the migmatite and marbles are synchronous, the microstructure does not reflect static recrystallization by grain growth but must have formed by a different mechanism. Associated minerals and deformation microstructures indicate that brittle boudins formed on the retrograde path during cooling and exhumation.

None of the outcrop scale deformation structures in the high grade marbles of the study area reflect the top-to-North shearing and vertical flattening that is dominant in the surrounding lithologies of the Naxos metamorphic core complex. E-W shortening is the main strain components for all described deformation structures. The extension direction evolves from vertical (lλ) to south vergent (sλ+ domino boudins) to horizontal (torn boudins) to north vergent (hairline).

The presented reconstruction of the multiphase boudinage is made possible by the exceptional outcrop conditions and highlights the immense wealth of information that can be gained from detailed analysis of boudinage structures.

Acknowledgements

This paper was prepared within the framework of the research project “BoDy—Boudinage Dynamik” UR 64/14-1 funded by the Deutsche Forschungsgemeinschaft (DFG).

References

Abe, S. and Urai, J. L.: Discrete element modeling of boudinage: Insights on rock rheology, matrix flow, and evolution of geometry, J. Geophys. Res., 117(B1), doi:10.1029/2011JB008555, 2012.

Alsop, G. I. and Holdsworth, R. E.: Sheath folds as discriminators of bulk strain type, J. Struct. Geol., 28(9), 1588–1606, 2006.

Alsop, G. I. and Holdsworth, R. E.: Flow perturbation folding in shear zones, Geol. Soc. Lond. Spec. Publ., 272(1), 75–101, 2007.

Andriessen, P. A. M., Boelrijk, N., Hebeda, E. H., Priem, H. N. A., Verdurnen, E. T. and Verschure, R. H.: Dating the events of metamorphism and granitic magmatism in the Alpine Orogen of Naxos (Cyclades, Greece), Contrib. Mineral. Petrol., 69(3), 215–225, 1979.

Angelier, J.: Essai sur la neotectonique et les derniers stades tarditectoniques de l’arc egeen et de l’Egee meridionale, Bull. Soc. Geol. Fr., 7(3), 651–662, 1977.

Avigad, D.: High-pressure metamorphism and cooling on SE Naxos (Cyclades, Greece), Eur. J. Mineral., 1309–1320, doi:10.1127/ejm/10/6/1309, 1998.

Avigad, D., Ziv, A. and Garfunkel, Z.: Ductile and brittle shortening, extension-parallel folds and maintenance of crustal thickness in the central, Tectonics, 20(2), 277–287, 2001.

Biot, M. A.: Theory of internal buckling of a confined multilayered structure, Geol. Soc. Am. Bull., 75(6), 563–568, 1964.

Bolhar, R., Ring, U. and Ireland, T. R.: Zircon in amphibolites from Naxos, Aegean Sea, Greece: origin, significance and tectonic setting, J. Metamorph. Geol. [online] Available from: http://onlinelibrary.wiley.com/doi/10.1111/jmg.12238/full, 2016.

Brichau, S., Ring, U., Ketcham, R. A., Carter, A., Stockli, D. and Brunel, M.: Constraining the long-term evolution of the slip rate for a major extensional fault system in the central Aegean, Greece, using thermochronology, Earth Planet. Sci. Lett., 241(1), 293–306, 2006.

Brun, J.-P., Faccenna, C., Gueydan, F., Sokoutis, D., Philippon, M., Kydonakis, K. and Gorini, C.: The two-stage Aegean extension, from localized to distributed, a result of slab rollback acceleration 1, Can. J. Earth Sci., 53(11), 1142–1157, 2016.

Buick, I. S.: Mylonite fabric development on Naxos, Greece, J. Struct. Geol., 13(6), 643–655, 1991.

Buick, I. S. and Holland, T. J. B.: The PTt path associated with crustal extension, Naxos, Cyclades, Greece, Geol. Soc. Lond. Spec. Publ., 43(1), 365–369, 1989.

Burkhard, M.: Calcite twins, their geometry, appearance and significance as stress-strain markers and indicators of tectonic regime: a review, J. Struct. Geol., 15(3), 351–368, doi:10.1016/0191-8141(93)90132-T, 1993.

Cao, S., Neubauer, F., Bernroider, M., Genser, J., Liu, J. and Friedl, G.: Low-grade retrogression of a high-temperature metamorphic core complex: Naxos, Cyclades, Greece, Geol. Soc. Am. Bull., 129(1–2), 93–117, 2017.

Casey, M., Dietrich, D. and Ramsay, J. G.: Methods for determining deformation history for chocolate tablet boudinage with fibrous crystals, Tectonophysics, 92, 211–239, doi:10.1016/0040-1951(83)90091-4, 1983.

Cobbold, P. R. and Quinquis, H.: Development of sheath folds in shear regimes, J. Struct. Geol., 2(1–2), 119–126, 1980.

Covey-Crump, S. J. and Rutter, E. H.: Thermally-induced grain growth of calcite marbles on Naxos Island, Greece, Contrib. Mineral. Petrol., 101(1), 69–86, 1989.

Duchene, S., Aissa, R. and Vanderhaeghe, O.: Pressure-temperature-time evolution of metamorphic rocks from Naxos (Cyclades, Greece): constraints from thermobarometry and Rb/Sr dating, Geodin. Acta, 19(5), 301–321, 2006.

Dürr, S., Altherr, R., Keller, J., Okrusch, M. and Seidel, E.: The median Aegean crystalline belt: stratigraphy, structure, metamorphism, magmatism, Alps Apennines Hell., 38, 455–476, 1978.

Ebert, A., Rieke-Zapp, D., Herwegh, M., Ramseyer, K., Gnos, E. and Decrouez, D.: Microstructures of coarse-grained marbles, analyzed using a new technique based on the bireflectance of calcite, Tectonophysics, 463(1), 175–184, doi:10.1016/j.tecto.2008.09.041, 2009.

Forster, M. and Lister, G.: Core-complex-related extension of the Aegean lithosphere initiated at the Eocene-Oligocene transition, J. Geophys. Res. Solid Earth, 114(B2), 2009.

Gautier, P., Brun, J.-P. and Jolivet, L.: Structure and kinematics of Upper Cenozoic extensional detachment on Naxos and Paros (Cyclades Islands, Greece), Tectonics, 12(5), 1180–1194, doi:10.1029/93TC01131, 1993.

Gautier, P., Brun, J.-P., Moriceau, R., Sokoutis, D., Martinod, J. and Jolivet, L.: Timing, kinematics and cause of Aegean extension: a scenario based on a comparison with simple analogue experiments, Tectonophysics, 315(1), 31–72, 1999.

Goscombe, B. D. and Passchier, C. W.: Asymmetric boudins as shear sense indicators—an assessment from field data, J. Struct. Geol., 25(4), 575–589, 2003.

Goscombe, B. D., Passchier, C. W. and Hand, M.: Boudinage classification: end-member boudin types and modified boudin structures, J. Struct. Geol., 26(4), 739–763, doi:10.1016/j.jsg.2003.08.015, 2004.

Grasemann, B., Schneider, D. A., Stöckli, D. F. and Iglseder, C.: Miocene bivergent crustal extension in the Aegean: Evidence from the western Cyclades (Greece), Lithosphere, L164.1, doi:10.1130/L164.1, 2011.

Harker, A.: IV.—On Local Thickening of Dykes and Beds by Folding, Geol. Mag., 6(2), 69–70, doi:10.1017/S0016756800175910, 1889.

Hinsbergen, D. J. and Schmid, S. M.: Map view restoration of Aegean–West Anatolian accretion and extension since the Eocene, Tectonics, 31(5), 2012.

Ingram, G. M. and Urai, J. L.: Top-seal leakage through faults and fractures: the role of mudrock properties, Geol. Soc. Lond. Spec. Publ., 158(1), 125–135, 1999.

Jansen, J. B. H.: Geological Map of Greece, Island of Naxos (1: 50,000), Inst. Geol. Miner. Resour. Athens, 1973.

Jansen, J. B. H.: Metamorphism on Naxos, Greece., 1977.

Jansen, J. B. H. and Schuiling, R. D.: Metamorphism on Naxos; petrology and geothermal gradients, Am. J. Sci., 276(10), 1225–1253, 1976.

John, B.E. & Howard, K.A., 1995. Rapid extension recorded by cooling-age patterns and brittle deformation, Naxos, Greece. Journal of Geophysical Research: Solid Earth ,100, 9969–9979

Jolivet, L. and Brun, J.-P.: Cenozoic geodynamic evolution of the Aegean, Int. J. Earth Sci., 99(1), 109–138, doi:10.1007/s00531-008-0366-4, 2010.

Jolivet, L., Brun, J.-P., Gautier, P., Lallemant, S. and Patriat, M.: 3D-kinematics of extension in the Aegean region from the early Miocene to the Present, insights from the ductile crust, Bull Soc Geol Fr, 165(3), 195–209, 1994.

Jolivet, L., Famin, V., Mehl, C., Parra, T., Aubourg, C., Hébert, R. and Philippot, P.: Strain localization during crustal-scale boudinage to form extensional metamorphic domes in the Aegean Sea, Geol. Soc. Am. Spec. Pap., 380, 185–210, 2004.

Jolivet, L., Faccenna, C., Huet, B., Lecomte, E., Labrousse, L., Denèle, Y., Le Pourhiet, L., Lacombe, O., Burov, E. B., Meyer, B. and others: Aegean tectonics, a record of slab-overriding plate interactions, in AGU Fall Meeting Abstracts. [online] Available from: http://adsabs.harvard.edu/abs/2010AGUFM.T13G..04J, 2010.

Jolivet, L., Faccenna, C., Huet, B., Labrousse, L., Le Pourhiet, L., Lacombe, O., Lecomte, E., Burov, E., Denele, Y., Brun, J.-P. and others: Aegean tectonics: Strain localisation, slab tearing and trench retreat, Tectonophysics, 597, 1–33, 2013.

Jolivet, L., Menant, A., Sternai, P., Rabillard, A., Arbaret, L., Augier, R., Laurent, V., Beaudoin, A., Grasemann, B. and Huet, B.: The geological signature of a slab tear below the Aegean, Tectonophysics, 659, 166–182, 2015.

Keay, S., Lister, G. and Buick, I.: The timing of partial melting, Barrovian metamorphism and granite intrusion in the Naxos metamorphic core complex, Cyclades, Aegean Sea, Greece, Tectonophysics, 342(3–4), 275–312, doi:10.1016/S0040-1951(01)00168-8, 2001.

Kenis, I., Urai, J.L., van der Zee, W., Hilgers, C. and Sintubin, M. (2005). Rheology of fine-grained siliciclastic rocks in the middle crust – evidence from a combined structural and numerical analysis. Earth and Planetary Science Letters 233:351-360.

KENIS Ilse & Manuel SINTUBIN (2007) About boudins and mullions in the Ardenne-eifel area GEOLOGICA BELGICA 10/1-2: 79-91.

Kruckenberg, S. C., Ferré, E. C., Teyssier, C., Vanderhaeghe, O., Whitney, D. L., Seaton, N. C. and Skord, J. A.: Viscoplastic flow in migmatites deduced from fabric anisotropy: An example from the Naxos dome, Greece, J. Geophys. Res. Solid Earth, 115(B9) [online] Available from: http://onlinelibrary.wiley.com/doi/10.1029/2009JB007012/full, 2010.

Kruckenberg, S. C., Vanderhaeghe, O., Ferré, E. C., Teyssier, C. and Whitney, D. L.: Flow of partially molten crust and the internal dynamics of a migmatite dome, Naxos, Greece, Tectonics, 30(3) [online] Available from: http://onlinelibrary.wiley.com/doi/10.1029/2010TC002751/full, 2011.

Lecomte, E., Jolivet, L., Lacombe, O., Denèle, Y., Labrousse, L. and Le Pourhiet, L.: Geometry and kinematics of Mykonos detachment, Cyclades, Greece: Evidence for slip at shallow dip, Tectonics, 29(5), 2010.

Lister, G. S., Banga, G. and Feenstra, A.: Metamorphic core complexes of Cordilleran type in the Cyclades, Aegean Sea, Greece, Geology, 12(4), 221, doi:10.1130/0091-7613(1984)12<221:MCCOCT>2.0.CO;2, 1984.

Llorens, M.-G., Bons, P. D., Griera, A. and Gomez-Rivas, E.: When do folds unfold during progressive shear?, Geology, 41(5), 563–566, 2013.

Lohest, M.: De l'origine des veines et des géodes des terrains primaires de Belgique, Ann Soc Géol Belg B, 36, 275–282, 1909.

Maeder, X., Passchier, C. W. and Koehn, D.: Modelling of segment structures: Boudins, bone-boudins, mullions and related single- and multiphase deformation features, J. Struct. Geol., 31(8), 817–830, doi:10.1016/j.jsg.2009.05.013 <http://dx.doi.org/10.1016/j.jsg.2009.05.013>), 2009.

Malandri, C., Soukis, K., Maffione, M., Özkaptan, M., Vassilakis, E., Lozios, S. and Hinsbergen, D. J. J. van: Vertical-axis rotations accommodated along the Mid-Cycladic lineament on Paros Island in the extensional heart of the Aegean orocline (Greece), Lithosphere, 9(1), 78–99, doi:10.1130/L575.1, 2017.

Martin, L., Duchêne, S., Deloule, E. and Vanderhaeghe, O.: The isotopic composition of zircon and garnet: a record of the metamorphic history of Naxos, Greece, Lithos, 87(3), 174–192, 2006.

Martin, L. A., Duchêne, S., Deloule, E. and Vanderhaeghe, O.: Mobility of trace elements and oxygen in zircon during metamorphism: consequences for geochemical tracing, Earth Planet. Sci. Lett., 267(1), 161–174, 2008.

Menant, A., Jolivet, L., Augier, R. and Skarpelis, N.: The North Cycladic Detachment System and associated mineralization, Mykonos, Greece: Insights on the evolution of the Aegean domain, Tectonics, 32(3), 433–452, 2013.

Mercier, J. L., Carey, E., Philip, H. and Sorel, D.: La néotectonique plio-quaternaire de l'arc égéen externe et de la mer Egée et ses relations avec la séismicité, Bull. Soc. Geol. Fr., 7(2), 355–372, 1976.

Papanikolaou, D.: Contribution to the geology of Aegean Sea: the island of Paros, Ann. Geol. Pays Hell., 30(1), 65–96, 1980.

Philippon, M., Brun, J.-P. and Gueydan, F.: Tectonics of the Syros blueschists (Cyclades, Greece): From subduction to Aegean extension, Tectonics, 30(4), TC4001, doi:10.1029/2010TC002810, 2011.

Philippon, M., Brun, J.-P. and Gueydan, F.: Deciphering subduction from exhumation in the segmented Cycladic Blueschist Unit (Central Aegean, Greece), Tectonophysics, 524–525, 116–134, doi:10.1016/j.tecto.2011.12.025, 2012.

Philippon, M., Brun, J.-P., Gueydan, F. and Sokoutis, D.: The interaction between Aegean back-arc extension and Anatolia escape since Middle Miocene, Tectonophysics, 631, 176–188, 2014.

Poisel, R., Kolenprat, B., Bertagnoli, M., Ahmadabadi, M., Grasemann, B. and Hödlmoser, N.: The rockslide hazard in the former quarry near Spitz and its foreland/Die Felssturzgefahr im ehemaligen Tagebau Spitz ad Donau und dessen Vorland, Geomech. Tunn., 9(5), 497–507, 2016.

Ramberg, H.: Natural and Experimental Boudinage and Pinch-and-Swell Structures, J. Geol., 63(6), 512–526, doi:10.1086/626293, 1955.

Ramsay, A. C.: The Geology of North Wales.Memoirs of the Geological Survey of Great Britain 3. [online] Available from: https://www.abebooks.co.uk/book-search/title/the-geology-of-north-wales/author/ramsay-a-c/ (Accessed 5 June 2017), 1881.

Ramsay, J. G.: Folding and Fracturing of Rocks., McGraw-Hill, New York, 568. Scientific Research Publish. [online] Available from: http://www.scirp.org/(S(351jmbntvnsjt1aadkposzje))/reference/ReferencesPapers.aspx?ReferenceID=1688431 (Accessed 6 June 2017), 1967.

Reber, J. E., Schmalholz, S. M. and Burg, J.-P.: Stress orientation and fracturing during three-dimensional buckling: Numerical simulation and application to chocolate-tablet structures in folded turbidites, SW Portugal, Tectonophysics, 493(1), 187–195, 2010.

Rey, P. F., Teyssier, C., Kruckenberg, S. C. and Whitney, D. L.: Viscous collision in channel explains double domes in metamorphic core complexes, Geology, 39(4), 387–390, 2011.

Ridley, J.: Parallel stretching lineations and fold axes oblique to a shear displacement direction—a model and observations, J. Struct. Geol., 8(6), 647–653, doi:10.1016/0191-8141(86)90070-2, 1986.

Ring, U. and Layer, P. W.: High-pressure metamorphism in the Aegean, eastern Mediterranean: Underplating and exhumation from the Late Cretaceous until the Miocene to Recent above the retreating Hellenic subduction zone, Tectonics, 22(3) [online] Available from: http://onlinelibrary.wiley.com/doi/10.1029/2001TC001350/full, 2003.

Ring, U., Glodny, J., Will, T. and Thomson, S.: The Hellenic subduction system: high-pressure metamorphism, exhumation, normal faulting, and large-scale extension, Annu. Rev. Earth Planet. Sci., 38, 45–76, 2010.

Schenk, O., Urai, J. L. and Evans, B.: The effect of water on recrystallization behavior and grain boundary morphology in calcite–observations of natural marble mylonites, J. Struct. Geol., 27(10), 1856–1872, doi:10.1016/j.jsg.2005.05.015, 2005.

Schenk, O., Urai, J. L. and Zee, W. van der: Evolution of boudins under progressively decreasing pore pressure –A case study of pegmatites enclosed in marble deforming at high grade metamorphic conditions, Naxos, Greece, Am. J. Sci., 307(7), 1009–1033, doi:10.2475/07.2007.03, 2007.

Schmalholz, S. M. and Maeder, X.: Pinch-and-swell structure and shear zones in viscoplastic layers, J. Struct. Geol., 37, 75–88, 2012.

Schmalholz, S. M., Schmid, D. W. and Fletcher, R. C.: Evolution of pinch-and-swell structures in a power-law layer, J. Struct. Geol., 30(5), 649–663, doi:10.1016/j.jsg.2008.01.002, 2008.

Seward, D., O. Vanderhaeghe, L. Siebenaller, S. Thomson, C. Hibsch, A. Zingg, P. Holzner, U. Ring, and S. Duchêne (2009), Cenozoic tectonic evolution of Naxos Island through a multi-faceted approach of fission-track analysis, Geological Society, London, Special Publications, 321(1), 179-196.

Siebenaller, L., Boiron, M.-C., Vanderhaeghe, O., Hibsch, C., Jessell, M. W., Andre-Mayer, A.-S., France-Lanord, C. and Photiades, A.: Fluid record of rock exhumation across the brittle–ductile transition during formation of a Metamorphic Core Complex (Naxos Island, Cyclades, Greece), J. Metamorph. Geol., 31(3), 313–338, doi:10.1111/jmg.12023, 2013.

Urai, J. L., Schuiling, R. D. and Jansen, J. B. H.: Alpine deformation on Naxos (Greece), Geol. Soc. Lond. Spec. Publ., 54(1), 509–522, 1990.

Van Noten, K. and Sintubin, M.: Linear to non-linear relationship between vein spacing and layer thickness in centimetre-to decimetre-scale siliciclastic multilayers from the High-Ardenne slate belt (Belgium, Germany), J. Struct. Geol., 32(3), 377–391, 2010.

Vanderhaeghe, O.: Structural development of the Naxos migmatite dome, Geol. Soc. Am. Spec. Pap., 380, 211–227, 2004.

Virgo, S., Abe, S. and Urai, J. L.: Extension fracture propagation in rocks with veins: Insight into the crack-seal process using Discrete Element Method modeling, J. Geophys. Res. Solid Earth, 118(10), 5236–5251, doi:10.1002/2013JB010540, 2013.

Virgo, S., Abe, S. and Urai, J. L.: The evolution of crack seal vein and fracture networks in an evolving stress field: Insights from Discrete Element Models of fracture sealing, J. Geophys. Res. Solid Earth, 119(12), 2014JB011520, doi:10.1002/2014JB011520, 2014.

Virgo, S., Heup, T., Urai, J. L. and Berlage, T.: Virtual Petrography (ViP)-A virtual microscope for the geosciences, in EGU General Assembly Conference Abstracts, vol. 18, p. 14669. [online] Available from: http://adsabs.harvard.edu/abs/2016EGUGA..1814669V, 2016.

Walcott, C. and White, S.: Constraints on the kinematics of post-orogenic extension imposed by stretching lineations in the Aegean region, Tectonophysics, 298(1), 155–175, 1998a.

Walcott, C. R. and White, S. H.: Constraints on the kinematics of post-orogenic extension imposed by stretching lineations in the Aegean region, Tectonophysics, 298(1–3), 155–175, doi:10.1016/S0040-1951(98)00182-6, 1998b.

Wijbrans, J. R. and McDougall, I.: Metamorphic evolution of the Attic Cycladic Metamorphic Belt on Naxos (Cyclades, Greece) utilizing 40Ar/39Ar age spectrum measurements, J. Metamorph. Geol., 6(5), 571–594, 1988.

Zulauf, G., Gutiérrez-Alonso, G., Kraus, R., Petschick, R. and Potel, S.: Formation of chocolate-tablet boudins in a foreland fold and thrust belt: A case study from the external Variscides (Almograve, Portugal), J. Struct. Geol., 33(11), 1639–1649, 2011a.

Zulauf, J. and Zulauf, G.: Coeval folding and boudinage in four dimensions, J. Struct. Geol., 27(6), 1061–1068, 2005.

Zulauf, J., Zulauf, G., Kraus, R., Gutiérrez-Alonso, G. and Zanella, F.: The origin of tablet boudinage: Results from experiments using power–law rock analogs, Tectonophysics, 510(3), 327–336, 2011b.

Solid Earth Discuss., https://doi.org/10.5194/se-2017-91
Manuscript under review for journal Solid Earth
Discussion started: 23 August 2017

Figure Captions

Figure 1:
Geological map of Naxos, modified after Jansen (1993), Vanderhage (2004) and Kruckenberg et al. (2011). The study area (red box) is located in the central high grade migmatic core of the Naxos metamorphic core complex.

Figure 2:
a) Overview of the study area with outcrop locations (1-35) in vicinity of Kinidaros (top right). The marble quarries stick out as white patches in the Geoeye satellite image. b) Excerpt of the geological map modified after Kruckenberg et al. (2011). Most outcrops visited in this study are situated in the central high strain zone of the migmatite complex. Internal foliation of the migmatite is shown with dashed lines.

Figure 3:
Excellent outcrop conditions in marble quarries allow for detailed observation of the boudinaged amphibolite at vertical and horizontal faces. All images contain a geologist for scale. a) view to the West on Mount Bolibas, hosting the largest quarry in the area (Loc 16 -29). b) Inside the Bolibas quarry, view to the south. The subvertical N-S striking amphibolites can be followed over all soles of the quarry. This section exposes mostly pinch and swell boudins. c) View to the west on an amphibolite surface (Loc 31). Layer parallel cuts like this are essential for age relationship observations and expose the subhorizontal necks of the lλ pinch and swell boudins, which are hard to identify in layer normal cuts. d) Recently abandoned quarry in the south of the field area (Loc 32-35) exposing many folds, brittle boudins and a large boudinaged inclusion of schist across a football field sized horizontal surface.

Figure 4:
Overview of the structures found in the study area and their orientation plotted in stereonets (lower hemisphere). Images on the left show typical examples of the structures in the field. Indicators highlight the component of the structure that is shown in the stereonet: Amphibolite layers are plotted as great circles (0). Pinch-and swell boudins (1,2) do not have boudin faces, therefore the long axis of the Boudin (L_b) is plotted. Folds are represented by their fold axis (3). The plane of the boudin face S_b is plotted for domino boudins (4), torn boudins (5) and hairline veins are shown as great circles.

Figure 5:
Examples of vertical wall exposures. a) Isoclinal folds and pinch and swell boudins in a wall close to Loc 7, view to the north. Banding of the marble is parallel to the amphibolite layers. b) Interference of lλ and sλ pinch and swell boudins. In layer normal 2D sections it is challenging to distinguish between the two generations (Loc 20, view to the south). c) E-W trending normal fault in the marble with a pronounced damage zone. The fault is filled with calcareous sinter (close to Loc 8, view to the east)

Figure 6:
a) Rare example of small scale concentric open folds in an amphibolite layer. much more common in the field area are asymmetric isoclinal folds. b) Isoclinal S-fold displaced by a late E-W trending oblique-slip fault. Both S and Z chiralities of folds are found in the study area. c) Fold axis orientations vary strongly (see also Fig. 4), here the axis plunges steeply to the north. The layer parallel cut of the limb exposes accumulations of biotite associated with the fold. d) S-fold with multiple

subfolds and increased amphibolite thickness in the limb (view to the west). Bright east-west trending hairline veins are parallel in the fold limbs and reef and not necessarily orthogonal to the amphibolite layer. e) Cuspate-lobate amphibolite-marble interfaces form foliation fans in some fold hinges. f) South dipping fold axis (dashed red line) in Loc 15. The apparent lineation on the thin exposed amphibolite layer (above the fieldbook) is parallel to lλ.

Figure 7:

Brittle boudinage structures are best observed on quarry floors. a) Multiple layers of amphibole with different boudin structures. The thin layers do not show any boudin structures while thicker layers boudinage in domino and torn boudins. The spacing of brittle boudins correlates with bed thickness, the lateral thickness variation results from older pinch and swell boudins. b) Adjacent pegmatite and amphibolite layer with synthetic domino boudins. The length of the boudins in the amphibolite is exceptionally long. c) Calcite and chlorite filled hairline veins crosscutting the shear planes of domino boudins. One of the fractures is an antithetic bending fracture. Usually the polarity of block rotation is very stable along a layer and antithetic fractures like this are rare in the study area. d) Lobate amphibolite interface in the limb of an asymmetric fold crosscut and displaced by shear fractures e) Torn boudins with slightly concave faces S_{ib}. A thin amphibolite layer highlights the deformation in the adjacent marble and shows the flow of marble into the interboudin zones. f) Chlorite filled mode-I hairline veins extending from the amphibolite layer into the surrounding marble.

Figure 8:

Micrographs of polished marble sections (thickness ~10-15 µm , crossed polarized light) illustrating the marble microstructure: a) The marble shows heterogeneous grain size, locally exceeding 10 mm. Extensive twinning indicates late low-temperature deformation. b) Top-left to bottom-right trending cluster of small scale shear zones in the marble associated with domino boudinage (compare Fig. 12). In the shear zone the grain size is strongly reduced. Adjacent calcites show undulouse extinction. c) Orientation families with similar extinction behavior are relicts of dynamically recrystallized larger grains. Lobate grain boundaries indicate high temperature grain boundary migration. d) Amphibole and plagioclase grains originating from the amphibolite on the right are intermingled with calcite grains in the neck of a pinch and swell boudin.

Figure 9:

Mined blocks frequently separate along amphibolite layers or their interfaces, exposing a planar view on the boudinage layers. Such outcrops allow for investigating the interaction of multiple boudinage generations. a) The subhorizontal long wavelength boudinage lλ is overprinted and slightly offset by the shorter wavelength boudinage sλ. The direction of sλ is consistent in the pinches and swells of lλ indicating sλ is younger (view to the east). b) Non in-situ block in a quarry split along a thin amphibolite layer. Domino boudins, torn boudins and hairline veins are clearly distinguishable. Torn boudins often terminate at the shear planes of domino boudins and at sλ pinches. Hairline veins crosscut all structures and are only locally deviated by preexisting domino shear planes. c) The interfering lλ and sλ pinch and swell boudins result in a variation of the amphibolite thickness across a layer, which is partly reflected by the local spacing of younger torn boudins (view to the east). d)Oblique view on an amphibolite marble interface. The pinches of lλ and sλ can be traced to an orthogonal cut in the neighboring wall, allowing for 3D inspection of the boudinaged layer. Remnants of slickensides can be locally found along the protruding faces of the domino boudins. e) Two sets of torn boudins interacting in a weathered-out amphibolite layer (view to the east).

Figure 10:

a) Sample of a folded amphibolite layer. red boxes show the thin section locations (b-d). Each section is shown in plane polarized light (left) and crossed polarized light (right). b) Cuspate-lobate structure in the fold hinge. Although significant

deformation can be expected in the lobes, the amphibolite shows no evidence of dynamic recrystallization. c) Biotite wraps around the interface of the amphibolite and into the pinched neck of this boudin. d) The calcitic inclusions in the fold hinge contain fragments of amphibole and indicate boudins prior to folding. The calcite grain size in the inclusions is consistently smaller than in the marble.

Figure 11:

a) Domino and torn boudins in a polished, 2 cm thick plate of marble. Close to the amphibolite layer the marble is more translucent. The transmitted light image highlights the shear zones extending from the domino boudins into the marble where they curve and splay. b) Overview of thin section locations of c, d and Fig. 12. The amphibolite layer is the same as shown in a. c) This torn boudin neck is fill mostly with calcite and contains a chloritic rim. Large grain size indicates that torn boudin necks form primarily as veins and not by intrusion of the surrounding marble. d) Torn boudin neck filled with chlorite containing small calcite filled veinlets.

12:

Neighbouring thin sections showing the localized deformation of a domino boudin (see Fig. 11 for location). a) In them marble ~2 cm away from the amphibolite numerous parallel shear zones can be found. Grains along the shear zones show intense twinning and undulouse extinction. b) At the interface of the amphibolite the shear zone have merged into a single slip zone; the fine grained calcite fill easily breaks out during thin section preparation. c) The shear zone is partly filled with biotite and an opaque mineral (presumably pyrite) along the boudin face. The calcite in the zone between the separated blocks is intensely twinned and shows undulouse extinction. Amphibole grains are heavily fractured.

Figure 13:

Overview of the results of this study in temporal relation to each other and to regional events. Note that only the relative order of events is considered and the time axis and temperature curve are not to scale. Results are grouped in rows, overlapping boxes are interpreted as contemporaneous. Data on temperature and regional events and structures are compiled from Buick and Holland (1991), Katzir (1999), Schenk et al. (2007), Kruckenberg et al. (2010,2011), and Cao et al. (2016).

Solid Earth Discuss., https://doi.org/10.5194/se-2017-91
Manuscript under review for journal Solid Earth
Discussion started: 23 August 2017

Figure 1:

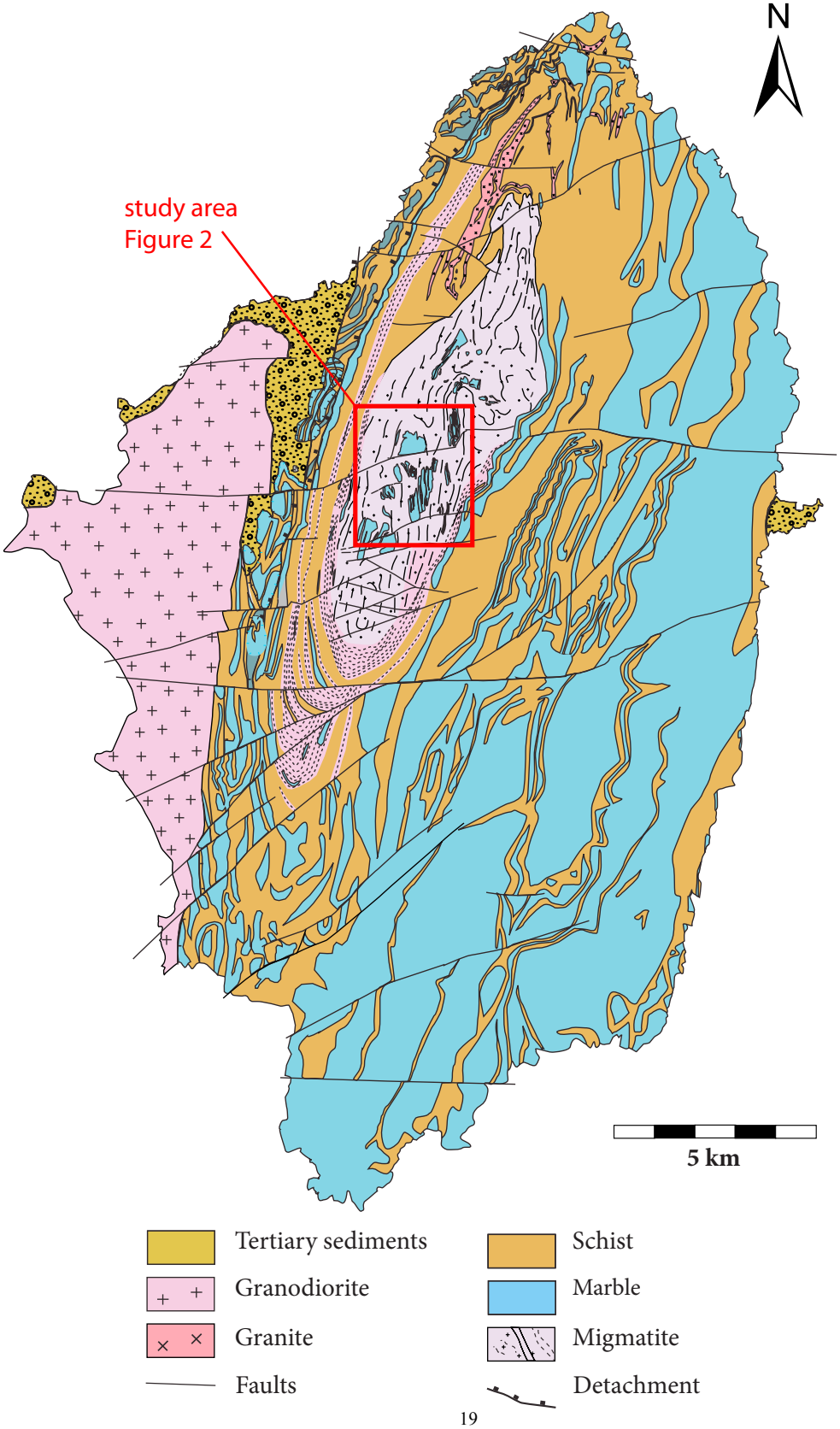

Solid Earth Discuss., https://doi.org/10.5194/se-2017-91
Manuscript under review for journal Solid Earth
Discussion started: 23 August 2017

Figure 2:

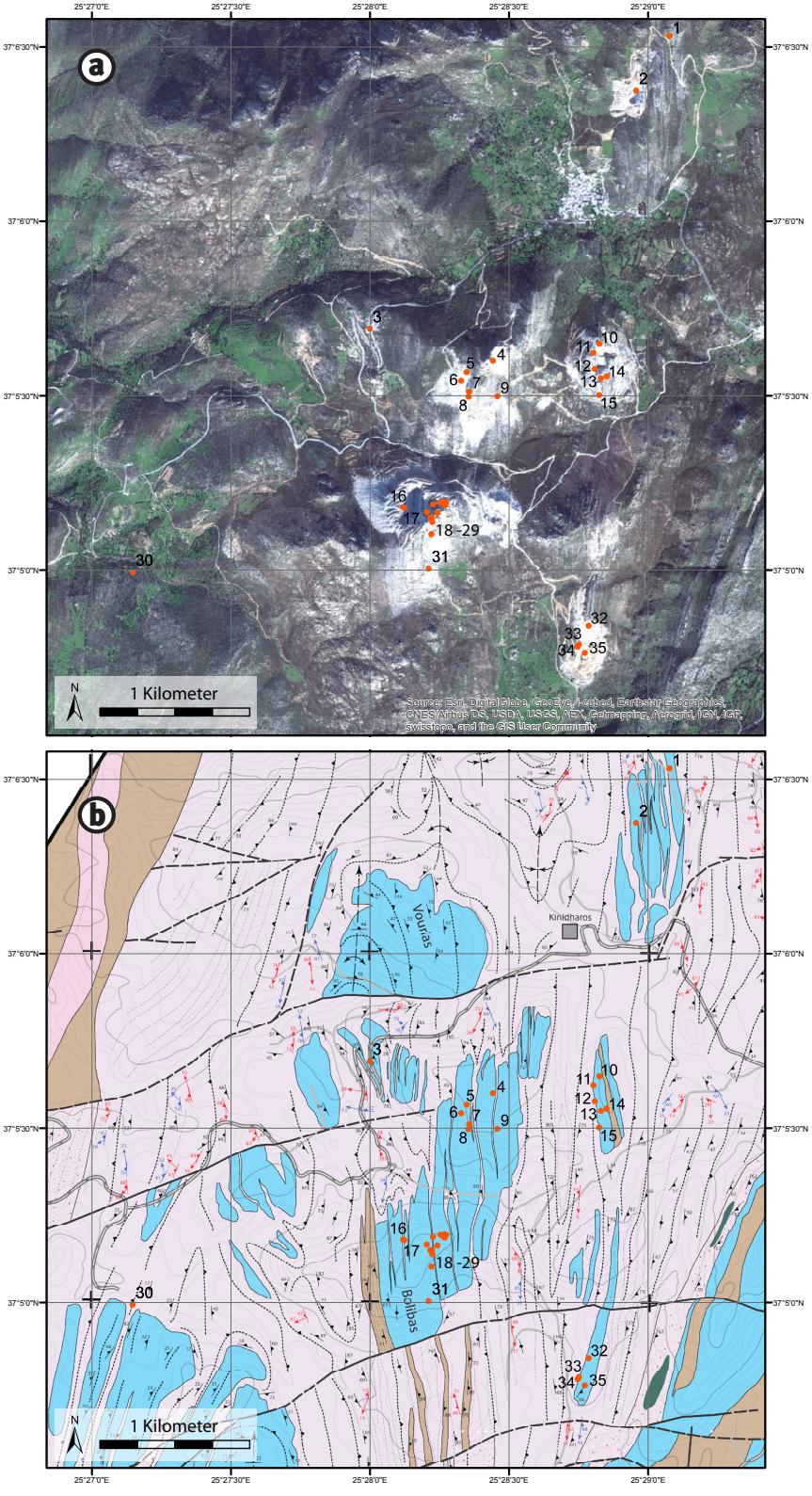

Solid Earth Discuss., https://doi.org/10.5194/se-2017-91
Manuscript under review for journal Solid Earth
Discussion started: 23 August 2017

Figure 3:

21

Solid Earth Discuss., https://doi.org/10.5194/se-2017-91
Manuscript under review for journal Solid Earth
Discussion started: 23 August 2017

Figure 4:

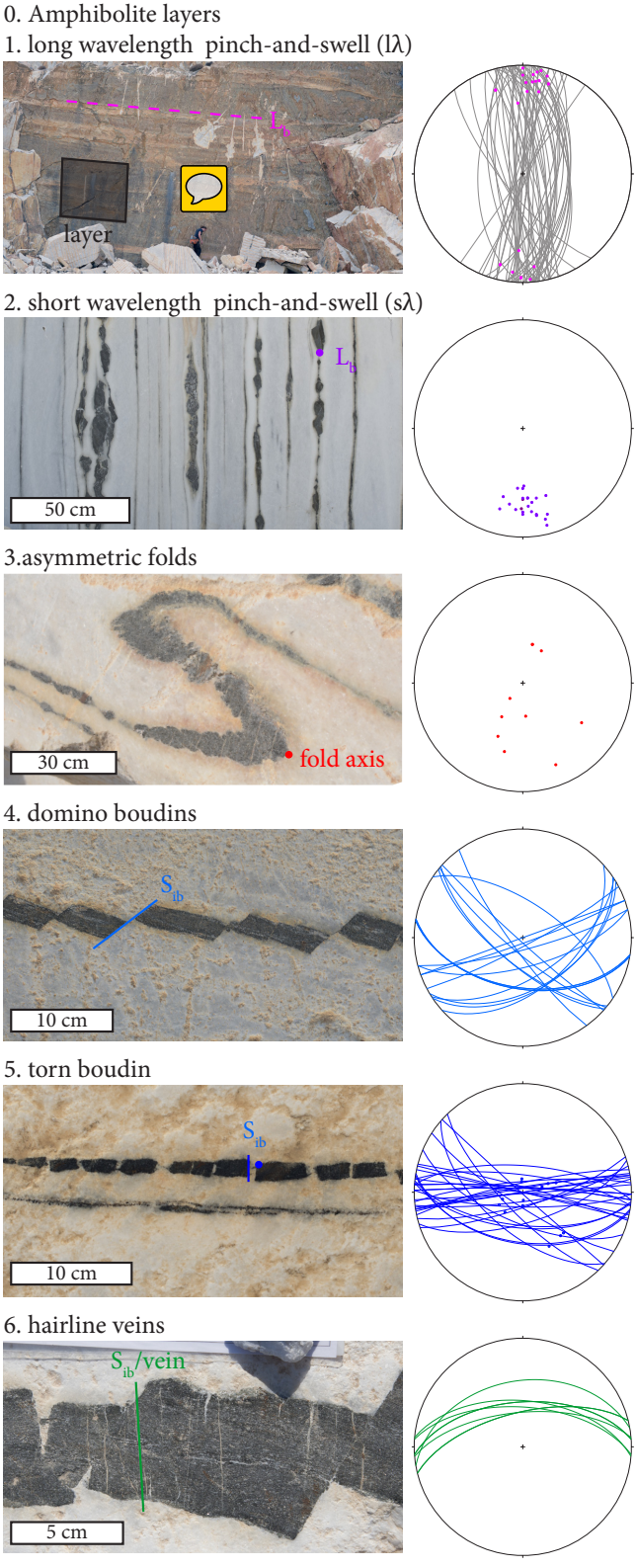

Solid Earth Discuss., https://doi.org/10.5194/se-2017-91
Manuscript under review for journal Solid Earth
Discussion started: 23 August 2017

Figure 5:

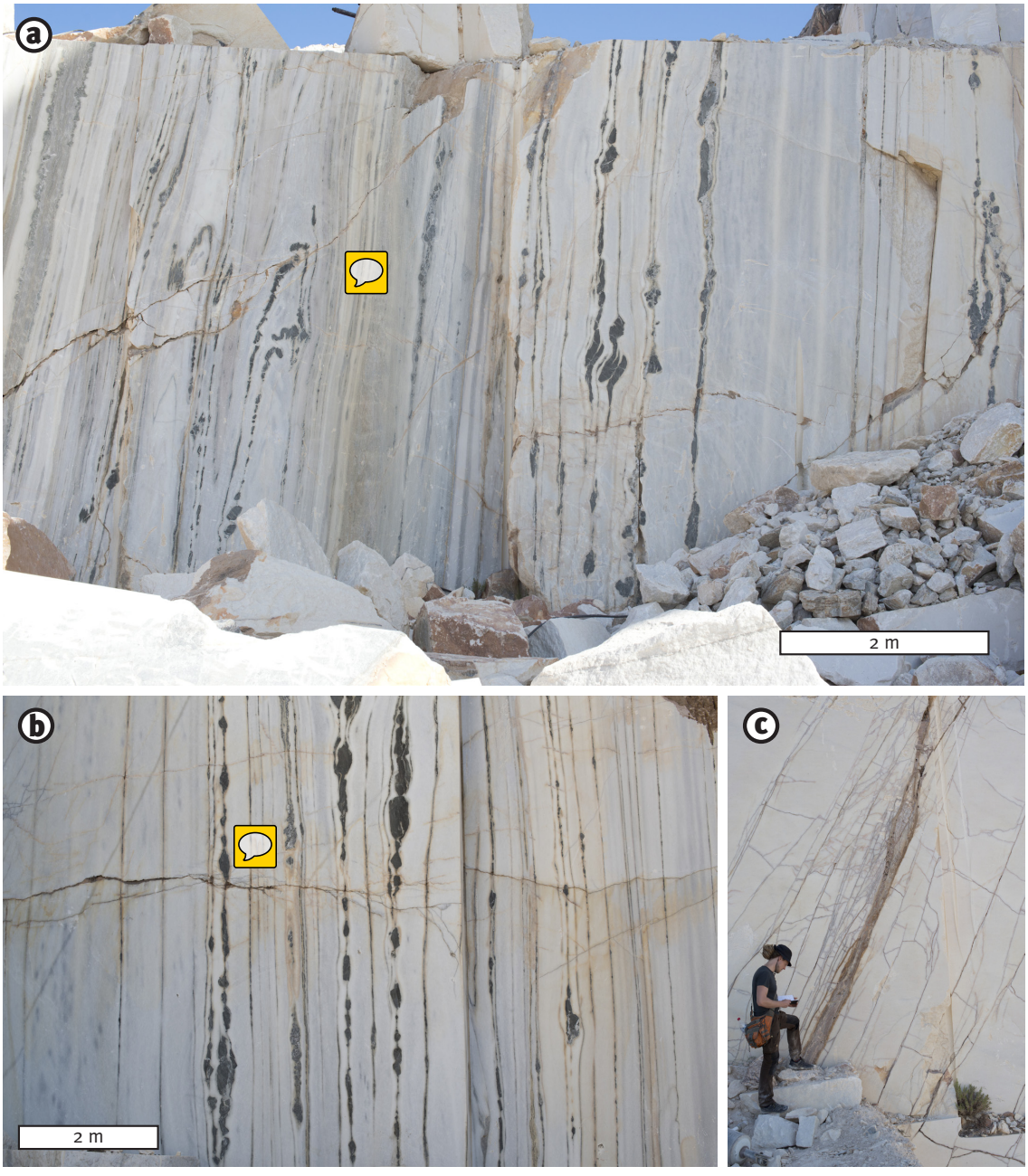

Solid Earth Discuss., https://doi.org/10.5194/se-2017-91
Manuscript under review for journal Solid Earth
Discussion started: 23 August 2017

Figure 6:

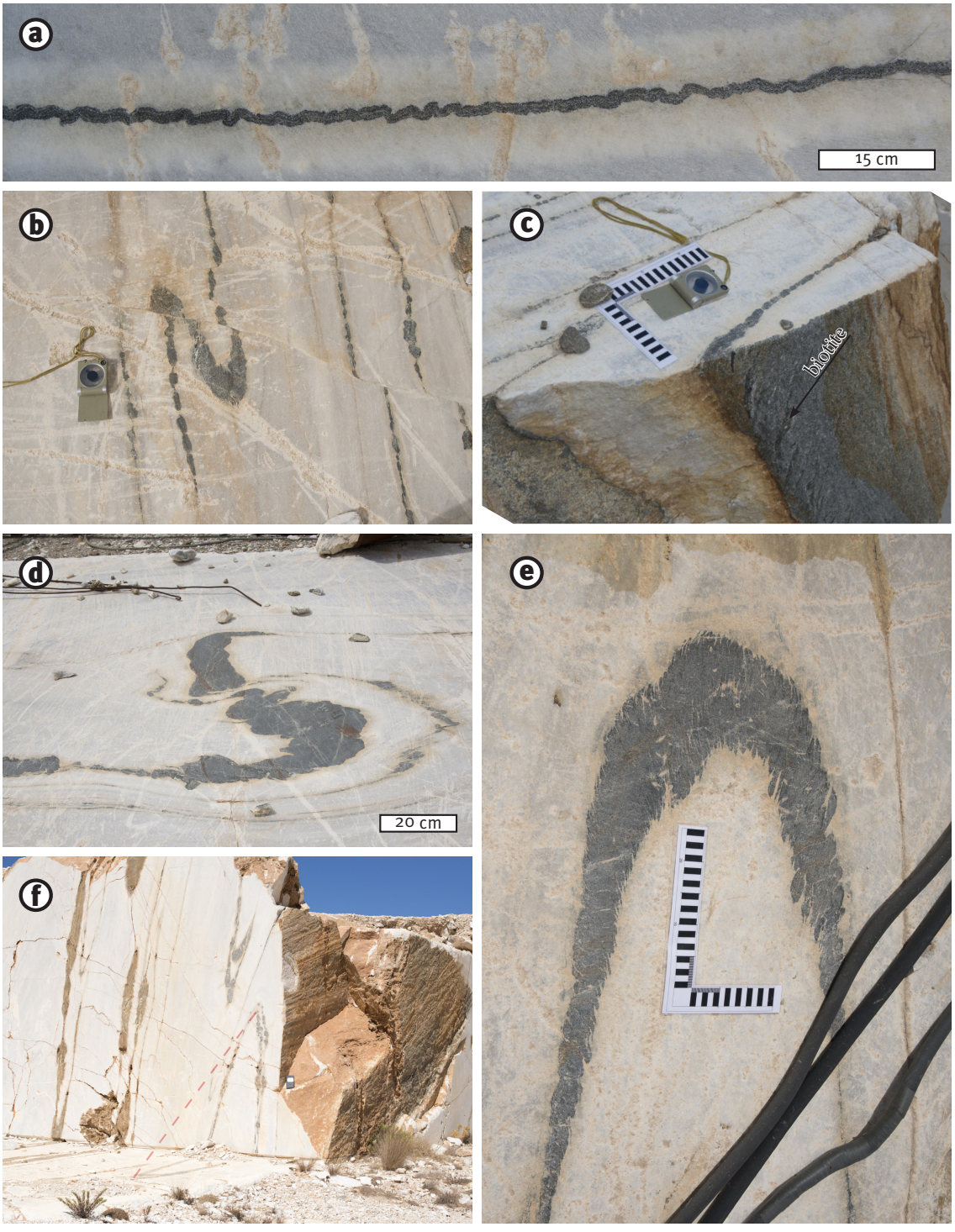

Solid Earth Discuss., https://doi.org/10.5194/se-2017-91
Manuscript under review for journal Solid Earth
Discussion started: 23 August 2017

Solid Earth Discussions
Open Access
EGU

Figure 7:

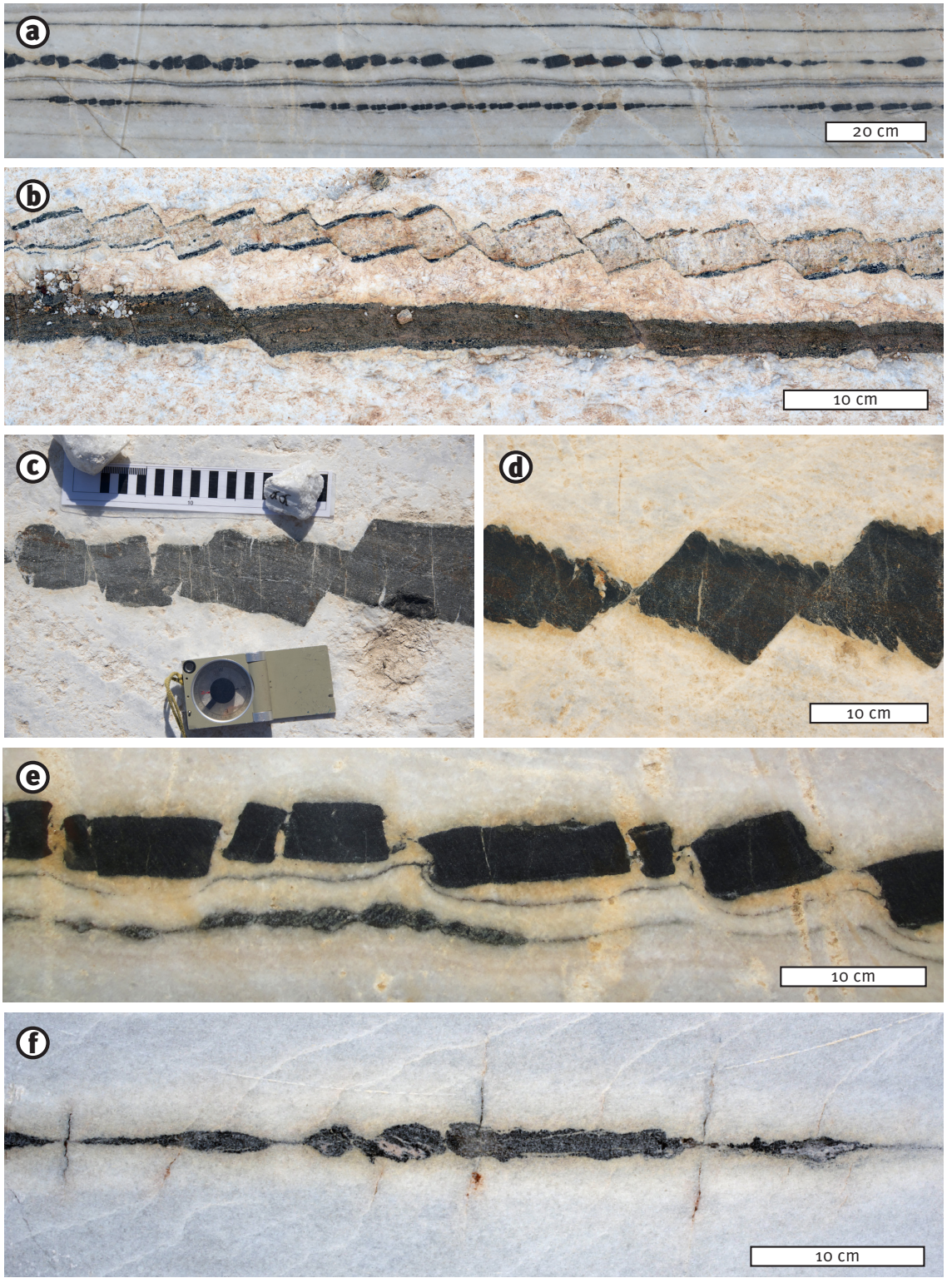

Solid Earth Discuss., https://doi.org/10.5194/se-2017-91
Manuscript under review for journal Solid Earth
Discussion started: 23 August 2017

Figure 8:

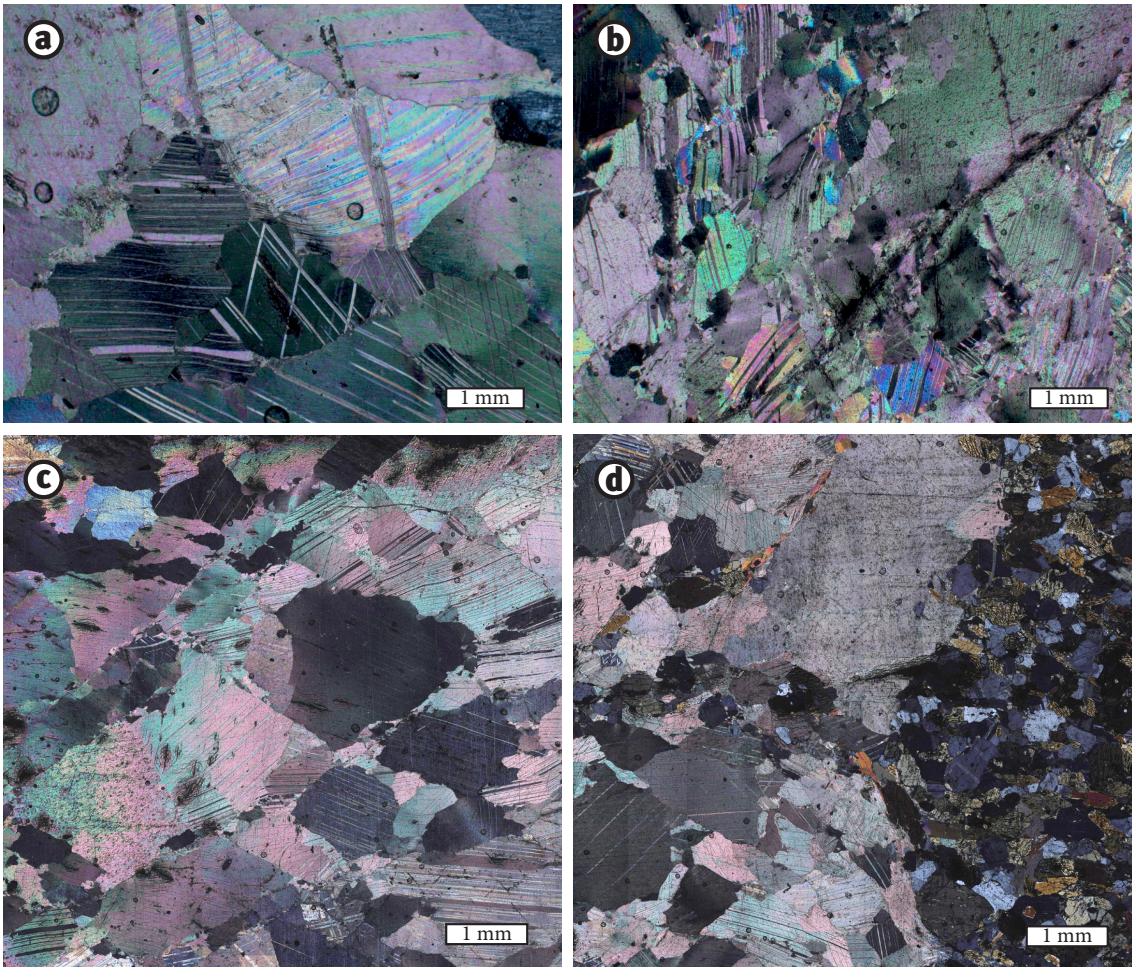

Solid Earth Discuss., https://doi.org/10.5194/se-2017-91
Manuscript under review for journal Solid Earth
Discussion started: 23 August 2017

Figure 9:

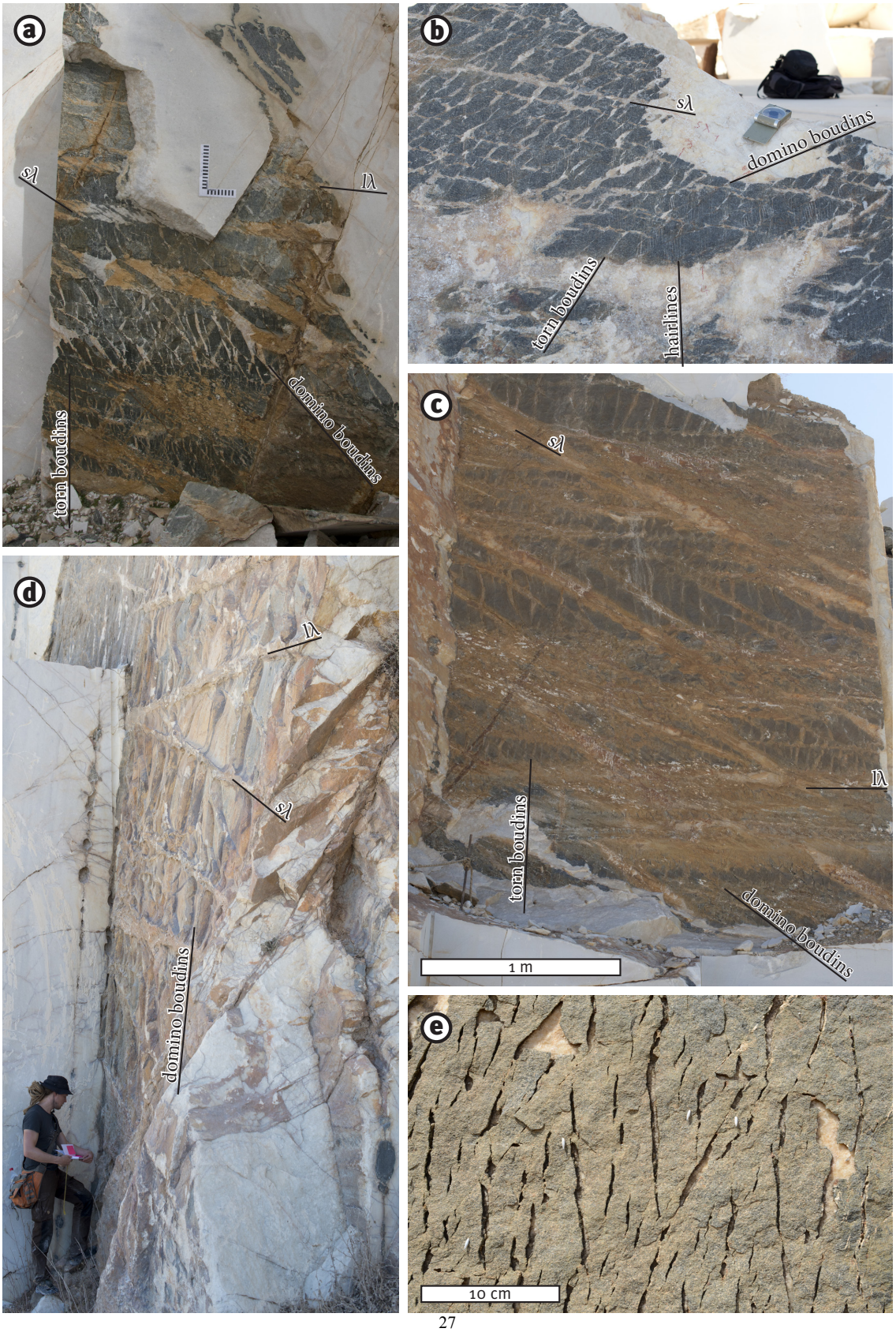

Solid Earth Discuss., https://doi.org/10.5194/se-2017-91
Manuscript under review for journal Solid Earth
Discussion started: 23 August 2017

Figure 10:

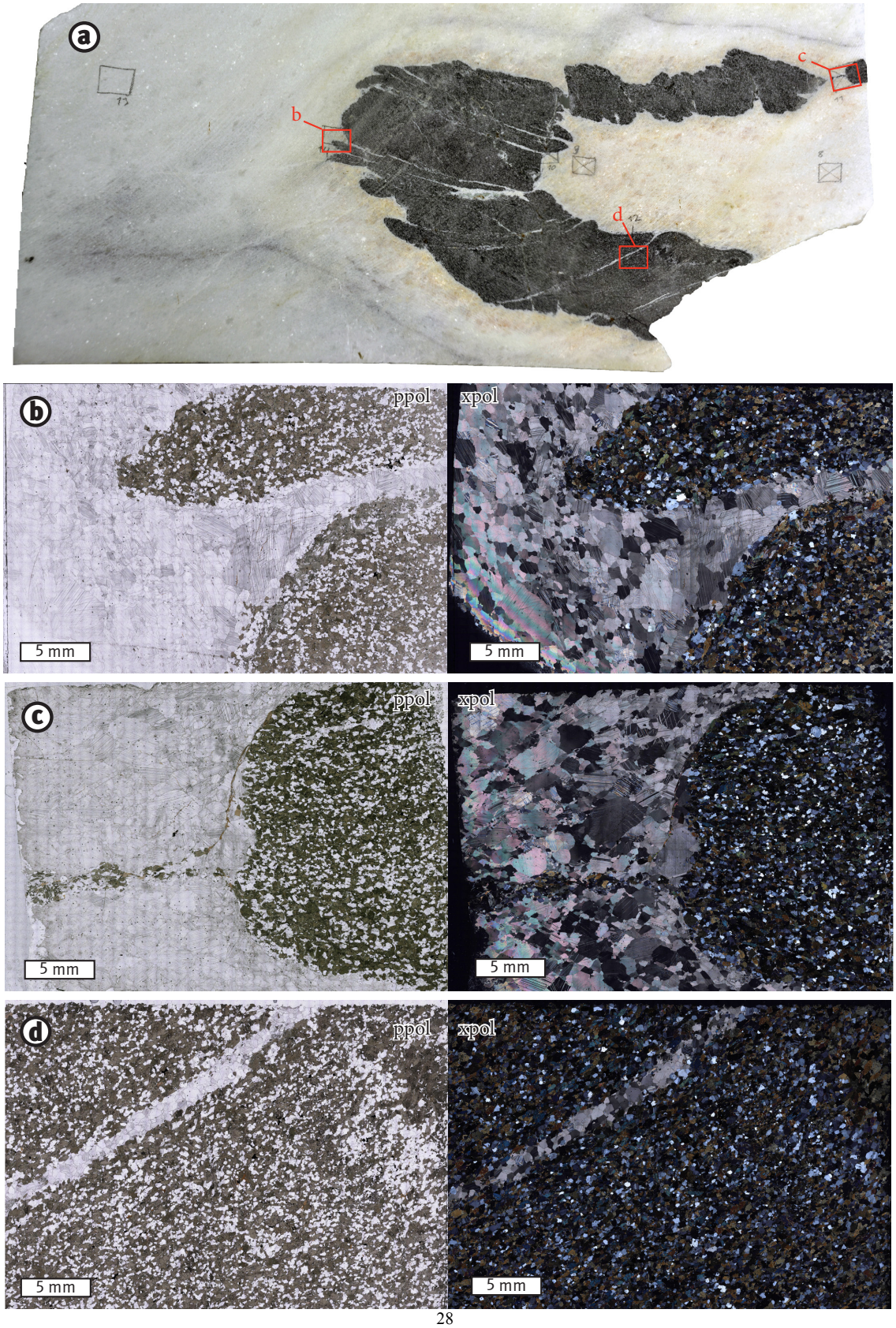

Solid Earth Discuss., https://doi.org/10.5194/se-2017-91
Manuscript under review for journal Solid Earth
Discussion started: 23 August 2017

Figure 11:

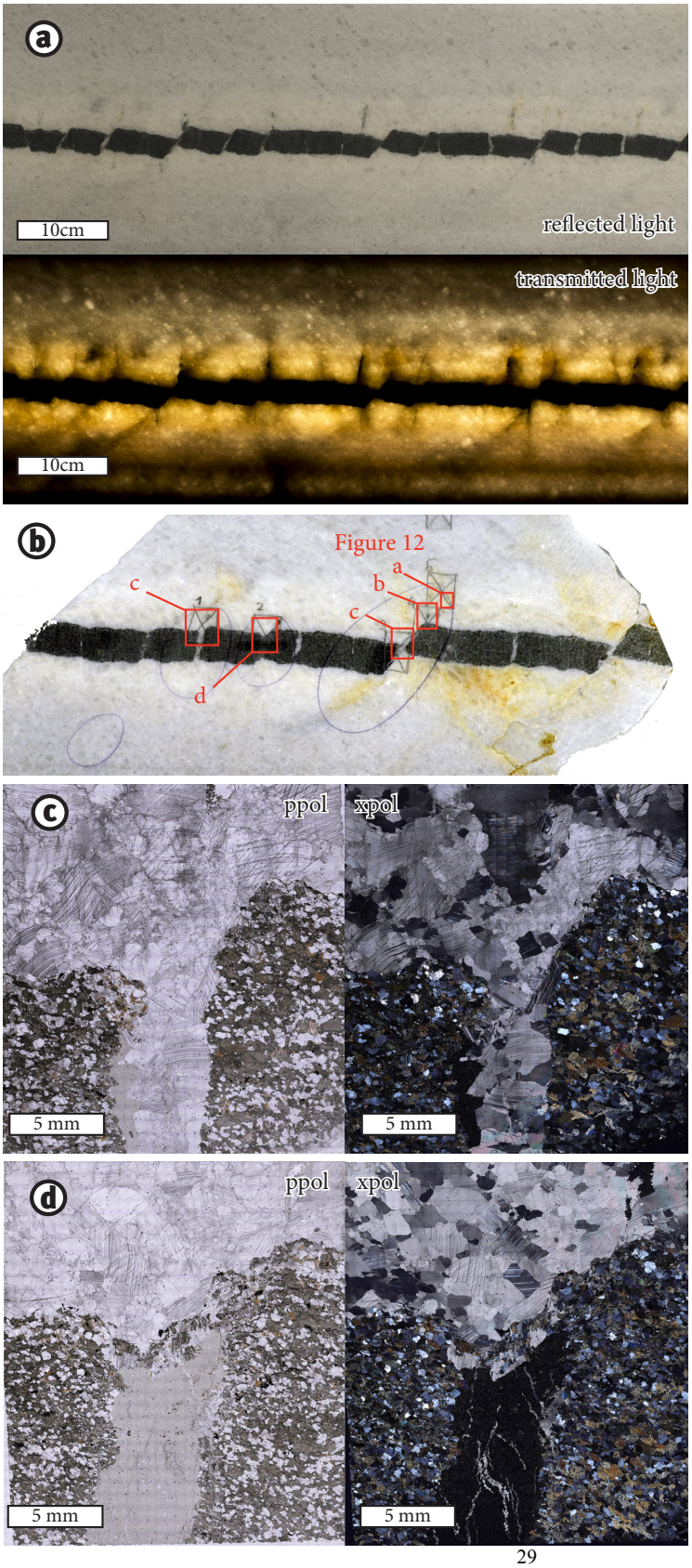

Solid Earth Discuss., https://doi.org/10.5194/se-2017-91
Manuscript under review for journal Solid Earth
Discussion started: 23 August 2017

Figure 12:

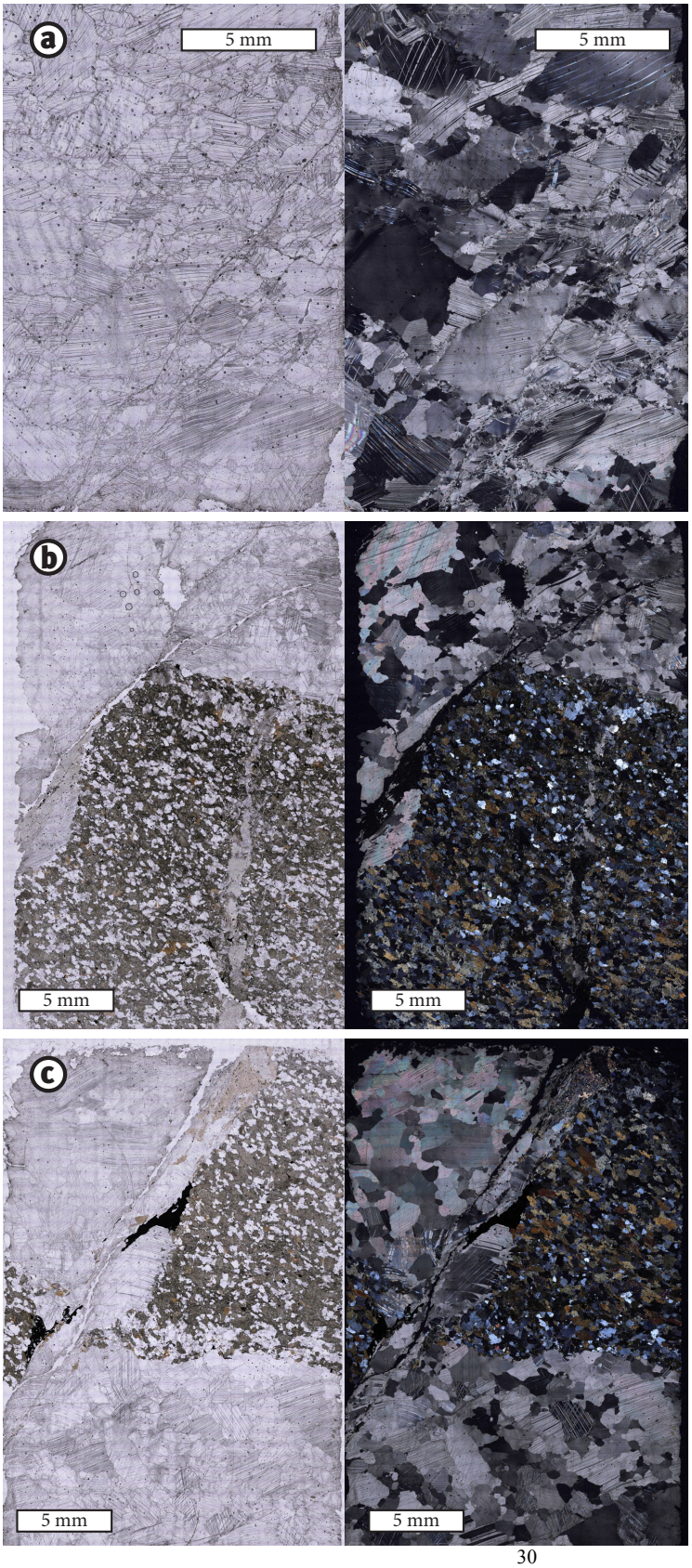

30

Solid Earth Discuss., https://doi.org/10.5194/se-2017-91
Manuscript under review for journal Solid Earth
Discussion started: 23 August 2017

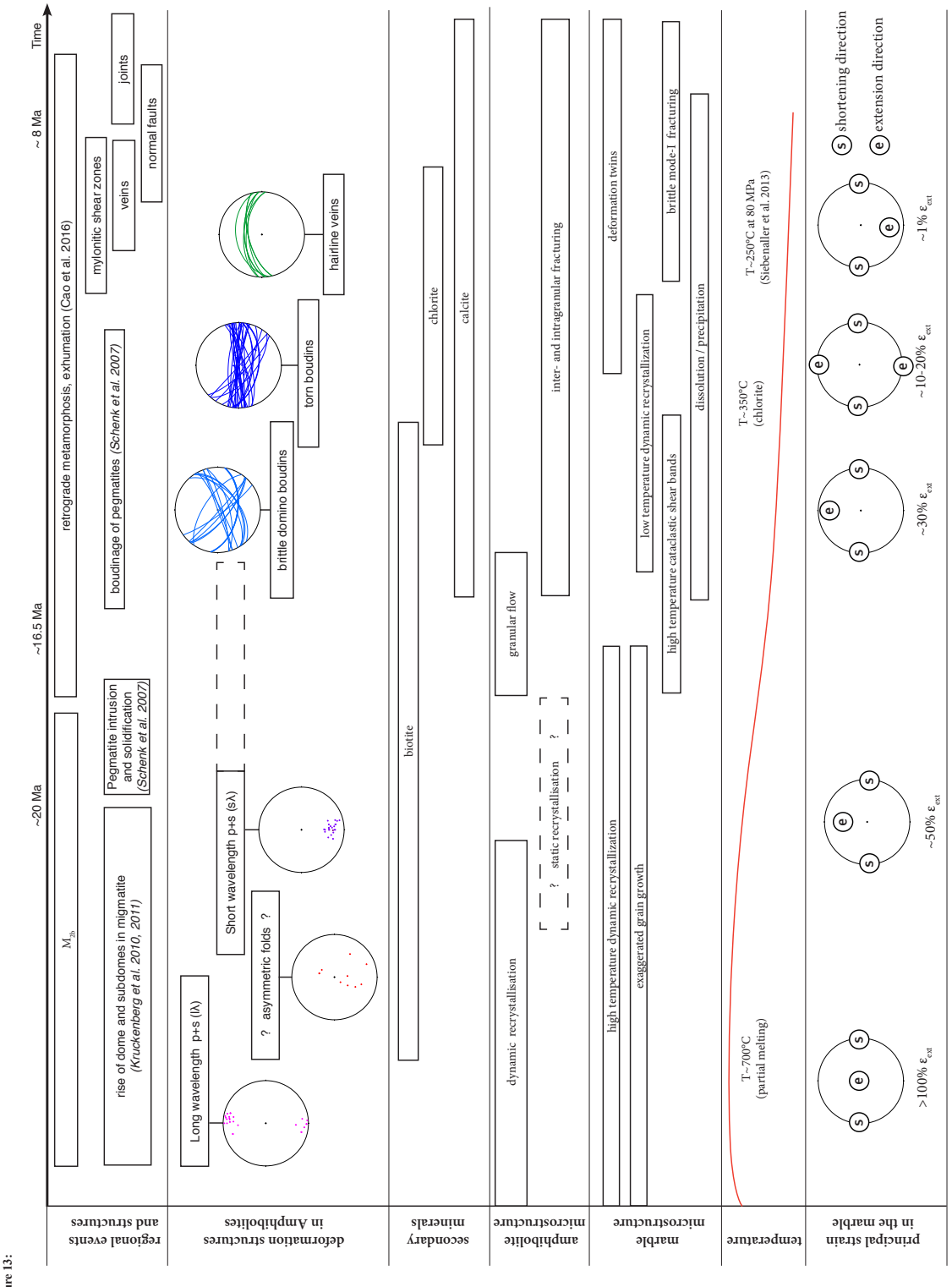

Figure 13: